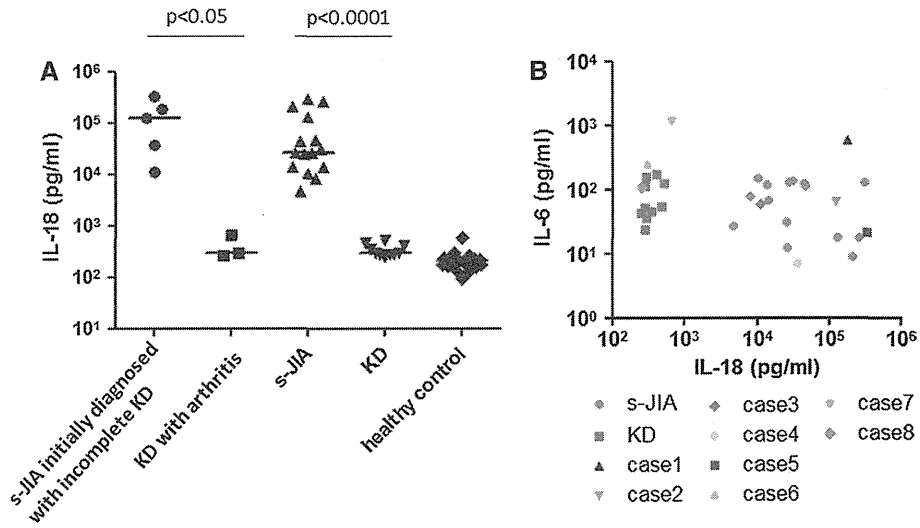

Fig. 1 Serum cytokine levels in patients with s-JIA and KD. **a** Serum IL-18 levels in patients with s-JIA and KD are shown. Bars represent median values. **b** s-JIA and KD are clearly divided into different subsets based on their serum IL-6 and IL-18 levels

met (although the presence of fever was required). The diagnosis of s-JIA was made in accordance with the criteria of the International League of Associations for Rheumatology [12]. Macrophage activation syndrome (MAS) was diagnosed on the basis of the combination of cytopenia affecting at least two-cell lineages, coagulopathy, and liver dysfunction, according to the guidelines proposed by Ravelli et al. [13].

The clinical characteristics of the patients in this study are shown in Table 1. All s-JIA patients (case 1–5) were diagnosed with incomplete KD on day 4–8 after onset of disease. Four patients had joint disease at the onset of s-JIA, but one patient had minimal joint disease, and the presence of arthritis was confirmed later. The patients received 2–5 courses of IVIG, but had no responses. All patients received plasma exchange and steroid therapy. Three patients (cases 1, 3, and 5) were treated with Tocilizumab. One patient (case 1) showed transient dilatation of coronary artery. One patient (case 5) was complicated with MAS.

Serum cytokine level measurements

Serum IL-18 and IL-6 levels were determined using commercial enzyme-linked immunosorbent assays according to the manufacturers' instructions (IL-18: MBL, Nagoya, Japan; IL-6: R&D Systems, Inc., Minneapolis, MN, USA).

Statistical analysis

The results are presented as mean ± SD. Comparison between the groups was made using the Mann–Whitney U test. Differences with $P < 0.05$ were considered statistically significant.

Results

As shown in Table 1, most of the symptoms overlapped between the s-JIA and KD groups; however, patients with s-JIA did not show redness or crust formation at the BCG inoculation site. Serum IL-18 levels in patients with s-JIA who were initially diagnosed with incomplete KD (median 123,000; range 10,860–330,000 pg/mL) were significantly elevated compared with those in patients with KD with arthritis [median, 298; range 260–660 pg/mL, $P < 0.05$; (Table 1 and Fig. 1a)]. Serum IL-6 levels in patients with KD with arthritis (median 250; range 106–1,200 pg/mL) were elevated compared with those in patients with s-JIA who were initially diagnosed with incomplete KD (median 58; range 7–580 pg/mL), although the difference was not statistically significant. As shown in Fig. 1b, the patients with s-JIA and KD were clearly divided into different subsets on the basis of their serum IL-6 and IL-18 levels.

Discussion

KD and s-JIA can be considered as potential differential diagnosis for prolonged fever, rash, and lymphadenopathy in children. In addition, clinical features of KD and s-JIA tend to overlap. Both diseases show similar laboratory findings such as elevated C-reactive protein level, leukocytosis, thrombocytosis, hypoalbuminemia, and anemia. Arthritis may occur in KD during the subacute and convalescent phase and is characteristically self-limited [2]. Even the dilation of coronary artery cannot be considered as definitive evidence to differentiate between these conditions because patients with s-JIA may also have coronary artery dilation similar to that observed in children with Kawasaki disease [5]. A poor response to IVIG and efficacy of steroid

therapy has been noted in KD patients [14]. These difficulties make the clinical diagnosis of these patients difficult, and at present, it is challenging for a pediatrician to diagnose the patients accurately.

IL-18 was originally described as an interferon-γ-inducing factor mainly produced by activated macrophagic cells [15]. IL-18 stimulates a variety of inflammatory responses. IL-18 enhances proliferation and activity of T cells and natural killer cells, shifts a T-cell balance toward T-helper 1 response [15]. We recently reported that serum levels of IL-18 are highly elevated in patients with s-JIA, and the abnormal production of IL-18 appears to be specific to s-JIA [10]. In this study, serum IL-18 levels were markedly elevated during the acute phase in patients with s-JIA who were initially diagnosed with incomplete KD, whereas IL-18 levels in patients diagnosed with complete KD and arthritis were within the reference range. These findings suggest that IL-18 may be an important mediator in s-JIA disease process, and serum IL-18 level may be a promising marker to differentiate s-JIA from KD.

It is still unclear whether KD acts as a trigger for s-JIA or the initial episode of KD is actually s-JIA in our case 1 because similar cases have been reported [6–9]. Both s-JIA and KD could share common triggering agents, susceptibility factors, or immunopathogenic pathways. In patients such as case 1, careful monitoring is necessary to prevent coronary aberrations and the development of macrophage activation syndrome.

In conclusion, pediatricians need to be aware that the presentation of s-JIA can mimic incomplete KD. Because the clinical features overlap, a high index of suspicion is warranted. The measurement of serum IL-18 can be useful for differentiating s-JIA from KD.

Acknowledgments We thank Harumi Matsukawa for technical assistance.

Conflict of interest The authors have no conflict of interest.

References

1. Abuhammour W, Yousef N (2008) Incomplete Kawasaki disease: experience with 14 patients with cardiac complications. J Pediatr Infect Dis 3:91–95
2. Gong GW, McCrindle BW, Ching JC, Yeung RS (2006) Arthritis presenting during the acute phase of Kawasaki disease. J Pediatr 148:800–805
3. Stabile A, Avallone L, Compagnone A, Ansuini V, Bertoni B, Rigante D (2006) Focus on juvenile idiopathic arthritis according to the 2001 revised Edmonton classification from the international league of associations for rheumatology: an Italian experience. Eur Rev Med Pharmacol Sci 10:229–234
4. Svantesson H, Bjorkhem G, Elborgh R (1983) Cardiac involvement in juvenile rheumatoid arthritis: a follow-up study. Acta Paediatr Scand 72:345–350
5. Binstadt BA, Levine JC, Nigrovic PA, Gauvreau K, Dedeoglu F, Fuhlbrigge RC et al (2005) Coronary artery dilation among patients presenting with systemic-onset juvenile idiopathic arthritis. Pediatrics 116:e89–e93
6. Dogra S, Gehlot A, Suri D, Rawat A, Kumar RM, Singh S (2013) Incomplete Kawasaki disease followed by systemic onset juvenile idiopathic arthritis- the diagnostic dilemma. Indian J Pediatr 80:783–785
7. Kumar S, Vaidyanathan B, Gayathri S, Rajam L (2013) Systemic onset juvenile idiopathic arthritis with macrophage activation syndrome misdiagnosed as Kawasaki disease: case report and literature review. Rheumatol Int 33:1065–1069
8. Rigante D, Valentini P, Onesimo R, Angelone DF, De Nisco A, Bersani G et al (2010) Incomplete Kawasaki syndrome followed by systemic onset-juvenile idiopathic arthritis mimicking Kawasaki syndrome. Rheumatol Int 30:535–539
9. Komatsu H, Tateno A (2007) Failure to distinguish systemic-onset juvenile idiopathic arthritis from incomplete Kawasaki disease in an infant. J Paediatr Child Health 43:707–709
10. Shimizu M, Yokoyama T, Yamada K, Kaneda H, Wada H, Wada T et al (2010) Distinct cytokine profiles of systemic-onset juvenile idiopathic arthritis-associated macrophage activation syndrome with particular emphasis on the role of interleukin-18 in its pathogenesis. Rheumatology (Oxford) 49:1645–1653
11. Newburger JW, Takahashi M, Gerber MA, Gewitz MH, Tani LY, Burns JC et al (2004) Diagnosis, treatment and long-term management of Kawasaki disease: a statement for health professionals from the committee on rheumatic fever, endocarditis and Kawasaki disease, council on cardiovascular disease in the young, American Heart Association. Pediatrics 114:1708–1733
12. Petty RE, Southwood TR, Manners P, Baum J, Glass DN, Goldenberg J et al (2004) International league of associations for rheumatology classification of juvenile idiopathic arthritis: second revision, Edmonton, 2001. J Rheumatol 31:390–392
13. Ravelli A, Magni-Manzoni S, Pistorio A, Besana C, Foti T, Ruperto N et al (2005) Preliminary diagnostic guidelines for macrophage activation syndrome complicating systemic juvenile idiopathic arthritis. J Pediatr 146:598–604
14. Lang BA, Yeung RS, Oen KG, Malleson PN, Huber AM, Riley M et al (2006) Corticosteroid treatment of refractory Kawasaki disease. J Rheumatol 33:803–809
15. Novick D, Kim S, Kaplanski G, Dinarello CA (2013) Interleukin-18, more than a Th1 cytokine. Semin Immunol 25:439–448

Defect of suppression of inflammasome-independent interleukin-8 secretion from SW982 synovial sarcoma cells by familial Mediterranean fever-derived pyrin mutations

Rino Sugiyama, Kazunaga Agematsu, Kiyoshi Migita, Jun Nakayama, Sho Mokuda, Fumiya Ogura, Kaho Haraikawa, Chikara Okumura, et

Molecular Biology Reports
An International Journal on Molecular and Cellular Biology

ISSN 0301-4851

Mol Biol Rep
DOI 10.1007/s11033-013-2890-y

ONLINE FIRST

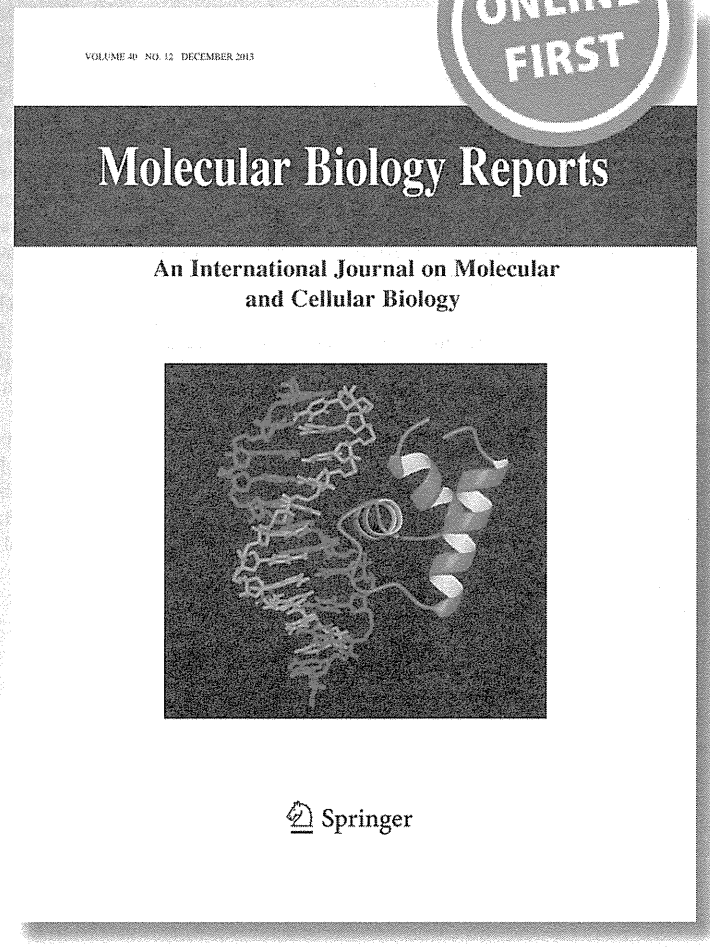

Springer

Mol Biol Rep
DOI 10.1007/s11033-013-2890-y

Defect of suppression of inflammasome-independent interleukin-8 secretion from SW982 synovial sarcoma cells by familial Mediterranean fever-derived pyrin mutations

Rino Sugiyama · Kazunaga Agematsu · Kiyoshi Migita · Jun Nakayama · Sho Mokuda · Fumiya Ogura · Kaho Haraikawa · Chikara Okumura · Satomi Suehiro · Shinnosuke Morikawa · Yuki Ito · Junya Masumoto

Received: 23 October 2012 / Accepted: 30 November 2013

Abstract Familial Mediterranean fever (FMF) is a recessive inherited autoinflammatory syndrome. Patients with FMF have symptoms such as recurrent fever and abdominal pain, sometimes accompanied by arthralgia. Biopsy specimens have revealed substantial neutrophil infiltration into synovia. FMF patients have a mutation in the Mediterranean fever gene, encoding pyrin, which is known to regulate the inflammasome, a platform for processing interleukin (IL)-1β. FMF patients heterozygous for E148Q mutation, heterozygous for M694I mutation, or combined heterozygous for E148Q and M694I mutations, which were found to be major mutations in an FMF study group in Japan, suffer from arthritis, the severity of which is likely to be lower than in FMF patients with M694V mutations. Expression plasmids of wild-type (WT) pyrin and mutated pyrin, such as E148Q, M694I, M694V, and E148Q+M694I, were constructed, and SW982 synovial sarcoma cells were transfected with these expression plasmids. IL-8 and IL-6 were spontaneously secreted from the culture supernatant of SW982 cells without any stimulation, whereas IL-1β and TNF-α could not be detected even when stimulated with lipopolysaccharide. Notably, two inflammasome components, ASC and caspase-1, could not be detected in SW982 cells by Western blotting. IL-8 but not IL-6 secretion from SW982 cells was largely suppressed by WT pyrin, but less suppressed by mutated pyrin, which appeared to become weaker in the order of E148Q, M694I, E148Q+M694I, and M694V mutations. As for IL-8 and IL-6, similar results were obtained using stable THP-1 cells expressing the WT pyrin or mutated pyrins, such as M694V or E148Q, when stimulated by LPS. In addition, IL-8 secretion from mononuclear cells of FMF patients was significantly higher than that of healthy volunteers when incubated on a culture plate. Thus, our results suggest that IL-8 secretion from SW982 synovial sarcoma cells suppressed by pyrin independently of inflammasome is affected by pyrin mutations, which may reflect the activity in FMF arthritis.

Keywords Pyrin · Familial Mediterranean fever · Interleukin-8 · Synovial sarcoma · SW982

R. Sugiyama · J. Nakayama · J. Masumoto
Department of Molecular Pathology, Shinshu University Graduate School of Medicine, Matsumoto, Nagano 390-8621, Japan

K. Agematsu
Department of Infectious Immunology, Shinshu University Graduate School of Medicine, Matsumoto, Nagano 390-8621, Japan

K. Migita
Clinical Research Center, Nagasaki Medical Center, Ōmura, Nagasaki 856-8562, Japan

S. Mokuda · F. Ogura · K. Haraikawa · C. Okumura · S. Suehiro · S. Morikawa · Y. Ito · J. Masumoto (✉)
Department of Pathology, Ehime University Proteo-Science Center and Graduate School of Medicine, Shitsukawa 454, Toon, Ehime 791-0295, Japan
e-mail: masumoto@m.ehime-u.ac.jp

Introduction

Familial Mediterranean fever (FMF) (OMIM#249100) is an autosomal recessive inherited autoinflammatory syndrome [1]. Patients with FMF have symptoms such as recurrent fever and abdominal pain, sometimes accompanied by arthralgia [1]. Patient biopsies have revealed that the cause is arthritis, involving neutrophils infiltrating into synovium [2]. Patients have a mutation in the Mediterranean fever (*MEFV*)

Published online: 07 December 2013

gene, encoding pyrin, which is known to regulate the inflammasome, a platform for processing interleukin (IL)-1β [3–5].

In Middle Eastern countries, FMF patients homozygous for M694V suffer a severe form of the disease, with clinical manifestations including arthritis, while the condition of FMF patients homozygous for M694I, one of the major mutations in Japan, is not so severe [6–8]. In Japan, there were no FMF patients with M694V mutation found by the Japan study group of FMF patients [9]. FMF patients heterozygous for E148Q, heterozygous for M694I, or combined-heterozygous for E148Q and M694I suffer from arthritis, and the severity of E148Q was reported to be lower than in FMF patients with M694V [10]. Interestingly, there was reported to be a corelationship between the concomitant expression of *MEFV* and C5a/IL-8-inhibitor activity in primary cultures of human fibroblasts [11].

Activation of inflammasome is reported to lead to IL-8 production from some cells, as well as that of IL-1β [12]. IL-8 is a chemotactic factor for neutrophils and enhances the trans-endothelial migration of neutrophils by inducing rapid shedding of L-selectin [13, 14]. Focal IL-8 secretion may reflect disease activity [15]. These facts prompted us to evaluate IL-8 secretion from synovial cells.

In this study, we evaluated the secretion of cytokines such as IL-1β, IL-6, IL-8, and TNF-α secretion from synovial sarcoma SW982 cells and monocytic leukemia THP-1 cells transfected with expression plasmids encoding wild-type (WT) pyrin and E148Q, M694V, M694I, and E148Q+M694I mutated pyrin in order to obtain new insight into FMF arthritis. Then, we also confirmed the results were reflected clinically in FMF patients.

Materials and methods

Preparation of expression plasmids

Expression plasmids encoding M694V, M694I, E148Q, E148Q+M694I, or WT pyrin were constructed as follows. The entire open reading frame of pyrin was inserted into the *EcoRI* and *BglII* sites of pFLAG-CMV-4 (Vector) (Sigma-Aldrich, St. Louis, MO, USA) to produce pFLAG-CMV-4-pyrin-WT from pcDNA3-HA-pyrin-WT as a template by polymerase chain reaction (PCR) using primer sets as follows: forward primer Pyrin-EcoRI-F 5-GCGAATTCAGCTAAGACCCCTAGTGACCAT-3 and reverse primer Pyrin-BglII-R 5-GTCAGATCTTCAGTCAGGCCCCTGACCACC-3 [16, 17]. PCR-based site-specific mutagenesis for pFLAG-CMV-4-pyrin-E148Q was generated by two-step PCR using primer sets as follows: forward primer Pyrin-EcoRI-F 5-GCGAATTCAGCTAAGACCCCTAGTGACCAT-3 and reverse primer Pyrin-E148Q-R 5-GGTGCAGCCAGCCCCAGGCCGGGAGGGGGC-3, and forward primer Pyrin-E148Q-F 5-GCCCCCTCCCGGCCTGGGGCTGGCTGCACC-3 and reverse primer Pyrin-BglII-R 5-GTCAGATCTTCAGTCAGGCCCCTGACCACC-3 for the first over-lapping DNA fragment set from pcDNA3-HA-pyrin-WT plasmid as a template [16, 17]. Full-length E148Q mutated-pyrin DNA fragment was amplified by second PCR using a primer set as follows: forward primer Pyrin-EcoRI-F 5-GCGAATTCAGCTAAGACCCCTAGTGACCAT-3 and reverse primer Pyrin-BglII-R 5-GTCAGATCTTCAGTCAGGCCCCTGACCACC-3 from the first over-lapping DNA fragment set as templates, and then inserted into the *EcoRI* and *BglII* sites of pFLAG-CMV-4. pFLAG-CMV-4-pyrin-M694V and pFLAG-CMV-4-pyrin-M694I were generated by the same method. pFLAG-CMV-4-pyrin-E148Q+M694I was also generated by the same method from pFLAG-CMV-4-pyrin-E148Q as a template. Primers and oligonucleotide sequences are listed in Table 1. Mutations were confirmed by sequencing (Fig. 1a).

Transfection of expression plasmids, their expression and generation of THP-1 stable cells

5×10^6 human embryonic kidney (HEK) 293T cells were transfected with 3 μg of pFLAG-CMV-4 (Vector), pFLAG-CMV-4-pyrin-WT, pFLAG-CMV-4-pyrin-E148Q, pFLAG-CMV-4-pyrin-M694I, pFLAG-CMV-4-pyrin-M694V, or pFLAG-CMV-4-pyrin-E148Q+M694I using the calcium phosphate method as described previously [18]. 36 h after transfection, each protein's expression was detected by Western blotting. 5×10^6 synovial sarcoma SW982 cells were transfected with pFLAG-CMV-4 (Vector), pFLAG-CMV-4-pyrin-WT, pFLAG-CMV-4-pyrin-E148Q, pFLAG-CMV-4-pyrin-M694I, pFLAG-CMV-4-pyrin-M694V, or pFLAG-CMV-4-pyrin-E148Q+M694I using Lipofectamine™ 2000 (Invitrogen, Grand Island, NY, USA) as per the manufacturer's instructions. 1×10^7

Table 1 Primers and oligonucleotide sequences for site-specific mutagenesis of pyrin plasmids

Name	Oligo-nucleotide-sequence
Pyrin-EcoRI-F	5′ GCGAATTCAGCTAAGACCCCTAGTGACCAT 3′
Pyrin-BglII-R	5′ GTCAGATCTTCAGTCAGGCCCCTGACCACC 3′
Pyrin-E148Q-F	5′GGTGCAGCCAGCCCCAGGCCGGGAGGGGGC 3′
Pyrin-E148Q-R	5′GCCCCCTCCCGGCCTGGGGCTGGCTGCACC 3′
Pyrin-M694I-F	5′GGTGGTGATAATGATCAAGGAAAATGAGTA 3′
Pyrin-M694I-R	5′TACTCATTTTCCTTGATCATTATCACCACC 3′
Pyrin-M694V-F	5′GGTGGTGATAATGGTGAAGGAAAATGAGTA 3′
Pyrin-M694V-R	5′TACTCATTTTCCTTCACCATTATCACCACC 3′

Underlines indicate mutation codons for specific amino acids

Double underlines indicate restriction enzyme sites

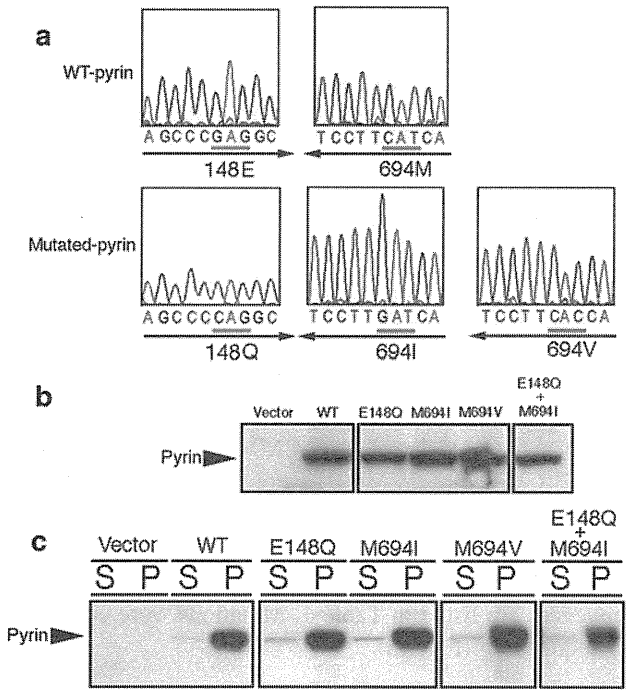

Fig. 1 Chart of sequencing of mutated pyrin plasmids, expression, and fractionation in human embryonic kidney 293T cells. **a** The mutated-pyrin expression plasmids pFLAG-CMV-4-pyrin E148Q, pFLAG-CMV-4-pyrin M694I, and pFLAG-CMV-4-pyrin M694V were sequenced to confirm (from GAG to CAG corresponding to E148Q; from complementary CAT to GAT corresponding to M694I; from complementary CAT to CAC corresponding to M694I) mutations in the appropriate site. **b** 5×10^6 human embryonic kidney 293T cells were transfected with 3 μg of pFLAG-CMV-4 (Vector), pFLAG-CMV-4-pyrin-WT, pFLAG-CMV-4-pyrin E148Q, pFLAG-CMV-4-pyrin-M694I, pFLAG-CMV-4-pyrin-M694V, and pFLAG-CMV-4-pyrin-E148Q+M694I. 36 h after transfection, 30 μg of each whole cell lysate was subjected to Western blotting. **c** 5×10^6 human embryonic kidney 293T cells were transfected with 3 μg of pFLAG-CMV-4 (Vector), pFLAG-CMV-4-pyrin-WT, pFLAG-CMV-4-pyrin E148Q, pFLAG-CMV-4-pyrin-M694I, pFLAG-CMV-4-pyrin-M694V, and pFLAG-CMV-4-pyrin-E148Q+M694I. 36 h after transfection, the cells were lysed in 1 % (v/v) NP-40 buffer and fractionated into soluble (*S* supernatant) and insoluble (*P* pellet) fraction. 30 μg of each fractionated protein was subjected to Western blotting

monocytic leukemia THP-1 cells were transfected with 5 μg of pFLAG-CMV-4 (Vector), pFLAG-CMV-4-pyrin-WT, pFLAG-CMV-4-pyrin-E148Q, or pFLAG-CMV-4-pyrin-M694V, using the Amaxa® Nucleofector as per the manufacturer's instructions. After incubation with 500 μg/ml G418 (Sigma) in RPMI 1640 medium including 10 % fetal bovine serum (FBS) (Defined, endotoxin ≦10 EU/ml; Thermo Scientific HyClone, South Logan, UT, USA) for 4 weeks at 37 °C in a humidified atmosphere with 5 % CO_2, THP-1 stable cells expressing WT or mutated pyrin protein were generated.

Fractionation of cell lysates

5×10^6 HEK293T cells were transfected with 3 μg of pFLAG-CMV-4 (Vector), pFLAG-CMV-4-pyrin-WT, pFLAG-CMV-4-pyrin-E148Q, pFLAG-CMV-4-pyrin-M694I, pFLAG-CMV-4-pyrin-M694V, and pFLAG-CMV-4-pyrin-E148Q+M694I. 36 h after transfection, the cells were lysed in 1.0 % (v/v) NP-40 buffer (1 % Nonidet P-40, 142.5 mM KCl, 5 mM MgCl–$6H_2O$, 10 mM HEPES [pH 7.6], 0.2 mM PMSF, 1 mM EDTA) with proteinase inhibitor cocktail Complete™ (Roche Molecular Biochemicals, Mannheim, Germany). The lysate was fully dislodged from the plate surface with a rubber policeman. The lysate from one dish was incubated in a 1.5-ml tube on ice, clarified by centrifugation at 12,000 rpm for 20 min, and separated into soluble (S: supernatant) and insoluble (P: pellet) fractions. Both fractions of the whole cell lysate were subjected to Western blotting using anti-pyrin polyclonal antibody (AL196; ALEXIS Biochemical, Lausen, Switzerland) (Fig. 1c).

Measurement of cytokine secretion from synovial sarcoma SW982 cells and monocytic leukemia THP-1 cells

Human synovial sarcoma SW982 cells and monocytic leukemia THP-1 cells were purchased from American Type Culture Collection, and pre-cultured in 12-well flat-bottomed plates (BD Biosciences, San Jose, CA, USA) to a final cell density of 1×10^6/ml in a volume of 1 ml of Dulbecco's modified Eagle's medium (DMEM; Invitrogen, Grand Island, NY, USA), including 10 % fetal FBS, for 24 h at 37 °C in a humidified atmosphere with 5 % CO_2. The cells in each well were transfected with 1.67 μg of expression plasmids in the presence of 0.67 μg of pEF1-BOS-β-gal. 8 h after transfection, culture medium was replaced by 1 ml of DMEM alone, or DMEM containing 1.0 ng/ml or 1.0 μg/ml of lipopolysaccharide (LPS) (from *Escherichia coli* O55:B5, cell culture tested, purified by phenol extraction; Sigma-Aldrich, St. Louis, MO, USA). 8 h after medium replacement, the concentrations of IL-1β, IL-6, IL-8, and TNF-α in the culture supernatant were measured by enzyme-linked immunosorbent assay (ELISA) with specific antibodies (BD Biosciences, San Jose, CA, USA). Percentiles of IL-8-related-suppression ratio of mutated pyrin versus WT pyrin were normalized to the transfection efficiency by β-galactosidase activity from triplicate experiments. THP-1-derived stable cells expressing WT or mutated pyrin proteins were pre-cultured in 24-well flat-bottomed plates (BD Biosciences, San Jose, CA, USA) to a final cell density of 2×10^7/ml in a volume

of 300 μl of RPMI1640 Medium (Invitrogen, Grand Island, NY, USA), including 10 % FBS, for 24 h at 37 °C in a humidified atmosphere with 5 % CO_2. Then, culture medium was replaced with 300 μl of RPMI1640 containing 10 ng/ml LPS. 8 h after medium replacement, the concentrations of IL-1β, IL-6, IL-8, and TNF-α in the culture supernatant were measured by ELISA with specific antibodies (BD Biosciences, San Jose, CA, USA).

Western blotting analyses for p38, ERK, and NF-κB pathways

40 μg of SW982 cell lysates were subjected to SDS-PAGE followed by Western blotting analysis for p38, ERK, and NF-κB, pathways. Signals from the same blotting membrane were detected by Phospho-p38 MAPK (Thr180/Tyr182) (D3F9) XP rabbit monoclonal antibody (Cell Signaling catalog No. #4511) and the p38α MAPK rabbit polyclonal antibody (Cell Signaling catalog No. #9218) for p38 MAPK pathway, or Phospho-p44/42 MAPK (Erk1/2) (Thr202/Tyr204) (D13.14.4E) XP rabbit monoclonal antibody (Cell Signaling catalog No. #4370) and p44/42 MAPK (Erk1/2) (137F5) rabbit monoclonal antibody (Cell Signaling catalog No. #4695) for the ERK pathway, or phospho-NF-κB p65 (Ser536) rabbit polyclonal antibody (Cell Signaling catalog No. #3031) and NF-κB p65 (D14E12) XP rabbit monoclonal antibodies (Cell Signaling catalog No. #8242) for the NF-κB pathway.

Cytokine assays for peripheral blood mononuclear cells

Participation of FMF patients and almost age-matched healthy volunteers regarding the analyses of *MEFV* gene and their blood samples with their written informed consents was approved by the institutional review board at the Shinshu University. We obtained peripheral blood mononuclear cells from five FMF patients with definite diagnosis as FMF according to the 'Tel Hashomer' criteria presented a symptom with typical type of FMF, and exhibited a favorable response to colchicine. All of them had *MEFV* mutations; four patients were E148Q/M694I compound heterozygotes (a 30-years-old woman, an 8-years-old boy, a 25-years-old woman and a 22-years-old woman) and one patient was an E148Q/E148Q homozygote (a 7-years-old girl). 5×10^5/ml of peripheral blood mononuclear cells were incubated in 96-well flat plates (Nunc) with RPMI1640 with 10 % heat-inactivated FBS for 6 h. The supernatants were collected and analyzed for cytokine concentration with the Cytometric Bead Array Flex set (BD Biosciences) according to the manufacturer's instructions. For intracellular cytokine staining, 5×10^5/ml of mononuclear cells including BD GolgiPlug protein transport inhibitor (BD Biosciences) were incubated under the same conditions as described above. After 6 h of incubation, adherent cells were collected by pipetting. The cells were fixed using a BD Cytofix/Cytoperm solution for 20 min at 4 °C, then the fixed cells were permeabilized by washing two times in 1 × BD Perm/Wash buffer. Intracellular IL-8 was stained with FITC-conjugated anti-IL-8 monoclona antibody (BioLegend) and APC-conjugated anti-IL-1β monoclona antibody (BioLegend) at 4 °C for 30 min. After washing with 1 × BD Perm/Wash buffer, resuspension in 1 × PBS was carried out, followed by flow cytometric analysis with a FACSCalibur flow cytometer.

Results

Mutated-pyrin expression plasmids were successfully constructed and expressed in HEK293T cells

Site-specific mutagenesis of plasmids, pFLAG-CMV-4-pyrin-E148Q, pFLAG-CMV-4-pyrin-M694I, pFLAG-CMV-4-pyrin-M694V, pFLAG-CMV-4-pyrin-E148Q+M694I, and pFLAG-CMV-4-pyrin-WT encoding E148Q, M694I, M694V, and E148Q+M694I mutated-pyrin and WT pyrin, generated from pcDNA3-HA-pyrin-WT as a template, was successfully completed and confirmed by sequencing (Fig. 1a). WT pyrin and E148Q, M694I, M694V, and E148Q+M694I mutated pyrin were stably expressed in HEK293T cells transfected with pFLAG-CMV-4-pyrin-WT, pFLAG-CMV-4-pyrin-E148Q, pFLAG-CMV-4-pyrin-M694I, pFLAG-CMV-4-pyrin-M694V, and pFLAG-CMV-4-pyrin-E148Q+M694I, whereas there was an undetectable level of pyrin in HEK293T cells transfected with pFLAG-CMV-4 (Vector) (Fig. 1b).

Wild-type pyrin and E148Q, M694I, M694V, and E148Q+M694I pyrin are detergent-insoluble

HEK293T cells were transfected with the expression plasmids pFLAG-CMV-4-pyrin-WT, pFLAG-CMV-4-pyrin-E148Q, pFLAG-CMV-4-pyrin-M694I, pFLAG-CMV-4-pyrin-M694V, or pFLAG-CMV-4-pyrin-E148Q+M694I, encoding WT, E148Q, M694I, M694V, and E148Q+M694I pyrin, respectively. The cells were suspended in 1.0 % NP-40 buffer and separated into soluble (S: supernatant) and insoluble (P: pellet) fractions by centrifugation at 12,000 rpm for 20 min. Both fractions were subjected to Western blotting. WT pyrin and all mutated pyrins that we tested were fractionated in detergent-insoluble fractions (Fig. 1c; P).

Cytokine secretion from synovial sarcoma SW982 cells

IL-8 and IL-6 were spontaneously secreted from synovial sarcoma SW982 cells (Fig. 2a, b), whereas IL-1β or TNF-α

could not be detected in our ELISA system even when stimulated by LPS (data not shown).

IL-8 secretion from SW982 cells was suppressed by WT pyrin but suppressed much less by mutated pyrins

When SW982 cells were transfected with expression plasmids pFLAG-CMV-4 (Vector), pFLAG-CMV-4-pyrin-E148Q, pFLAG-CMV-4-pyrin-M694I, pFLAG-CMV-4-pyrin-M694V, pFLAG-CMV-4-pyrin-E148Q+M694I, and pFLAG-CMV-4-pyrin-WT, IL-8 but not IL-6 secretion from SW982 seemed to be suppressed (Fig. 2a, b). After standardation to the β-galactosidase activity, related % of IL-8 secretion versus WT pyrin suppression, IL-8 secretion was significantly suppressed by WT pyrin but suppressed much less by E148Q, M694I, M694V, and E148Q+M694I pyrin in that order (Fig. 2c). In terms of IL-6 secretion from SW982 cells, there was no significant difference among all the mutations (Fig. 2d).

Neither ASC nor caspase-1 was expressed in 982 synovial sarcoma cells

The expressions of inflammasome components ASC and caspase-1 were analyzed by Western blotting. Although both ASC and caspase-1 were expressed in THP-1 monocytic leukemia cells, they were not expressed in SW982 cells as well as HEK293T cells (Fig. 3).

IL-1β, IL-8, TNF-α but not IL-6 secretion from THP-1 cells was suppressed by stably expressed WT pyrin but suppressed much less by stably expressed mutated pyrin proteins

We generated stable THP-1 cells transfected with expression plasmids pFLAG-CMV-4 (Vector), pFLAG-CMV-4-pyrin-E148Q, pFLAG-CMV-4-pyrin-M694 V, and pFLAG-CMV-4-pyrin-WT, which express no pyrin (vector control), or stably express mutant pyrin proteins such as M694V, E148Q, or WT pyrin (Fig. 4a inset). These cells secreted IL-

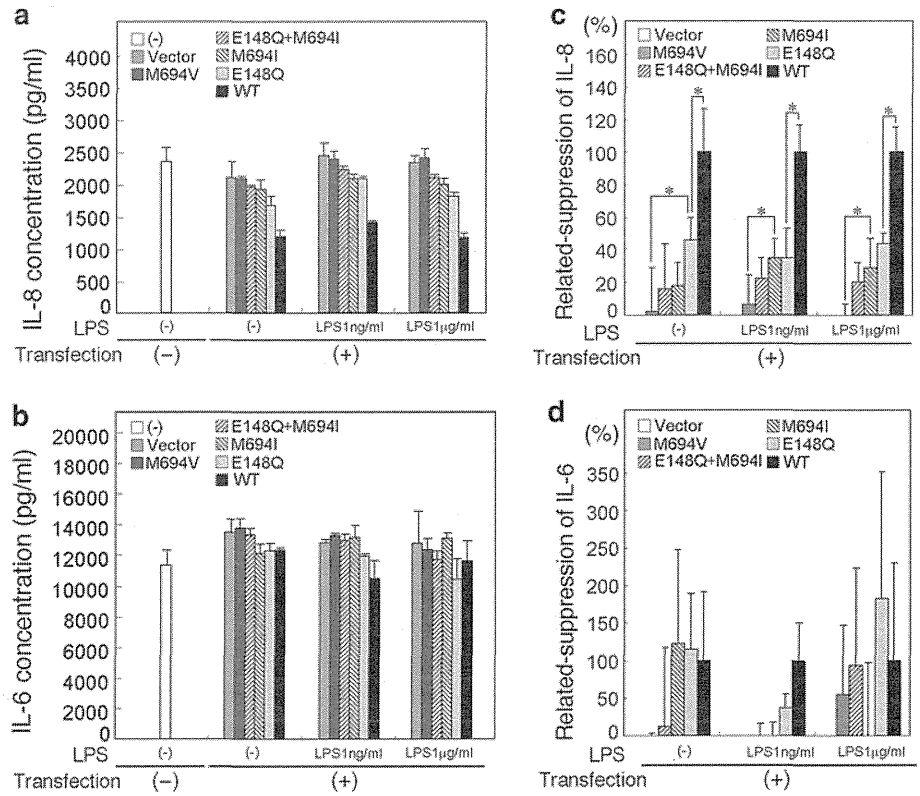

Fig. 2 Interleukin-8 and interleukin-6 secretion from SW982 synovial sarcoma cells transfected with expression plasmids. **a**, **b** 1×10^6 SW982 cells were transfected with 1.67 μg of pFLAG-CMV-4 (Vector), pFLAG-CMV-4-pyrin-M694V (M694V), pFLAG-CMV-4-pyrin-E148Q+M694I (E148Q+M694I), pFLAG-CMV-4-pyrin-M694I (M694I), pFLAG-CMV-4-pyrin-E148Q (E148Q), pFLAG-CMV-4-pyrin-WT (WT), or left untransfected (−) in the presence of 0.67 μg of pEF1-BOS-β-gal. 8 h after transfection, culture medium was replaced with 1 ml of DMEM alone [LPS(−)], or DMEM containing 1.0 ng/ml or 1.0 μg/ml LPS. 8 h after medium replacement, concentrations of interleukin-8 (IL-8) (**a**) and interleukin-6 (IL-6) (**b**) in the culture supernatant were measured by ELISA. Values are from triplicate cultures. **c**, **d** Percentiles are relative suppression of mutated pyrin versus WT pyrin. Percentiles of relative suppression of IL-8 (**c**) or IL-6 (**d**) secretion from SW982 cells transfected with mutated pyrin versus WT pyrin were normalized to the transfection efficiency by β-galactosidase activity from triplicate cultures. *A p value <0.05 was considered statistically significant

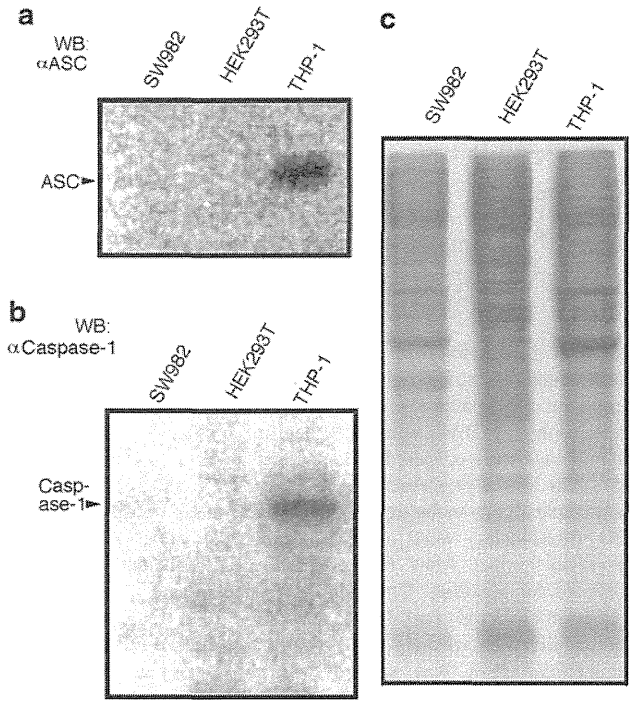

Fig. 3 Expression of ASC and caspase-1 in THP-1 cells, SW982 cells, and HEK293T cells by Western blotting analysis. Thirty μg of whole cell lysates of THP-1 cells, SW982 cells, and HEK293 cells was subjected to Western blotting. **a** Blotting membranes were detected using mouse anti-human ASC monoclonal antibody [26]. **b** Blotting membranes were detected using rabbit anti-human caspase-1 polyclonal antibody (Cell Signaling Technology, Danvers, MA, USA). **c** Gel was stained with Coomassie Brilliant Blue

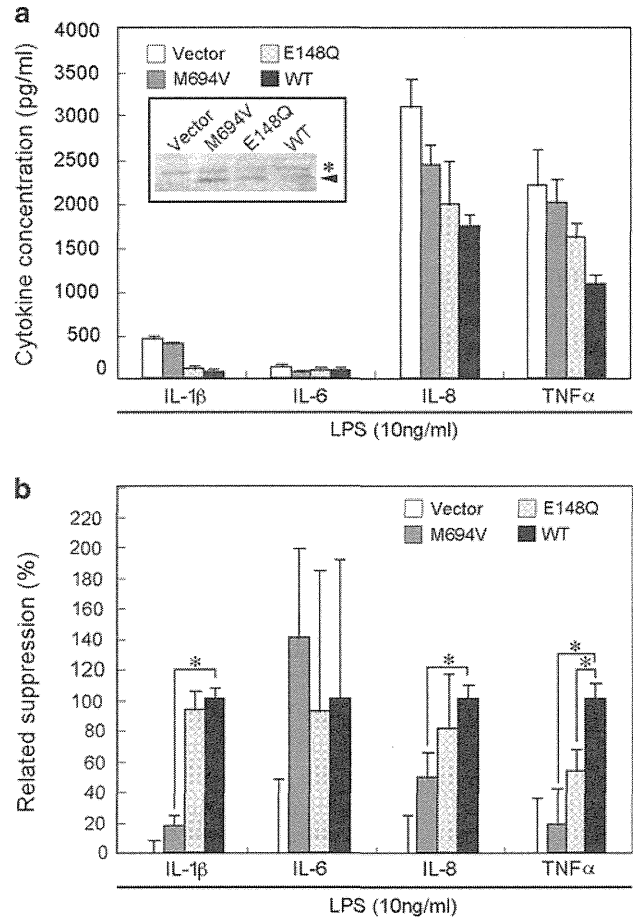

Fig. 4 Interleukin 1β, interleukin-6, interleukin-8, and TNF-α secretion from stable THP-1 cells. **a** 1×10^7 monocytic leukemia THP-1 cells were transfected with 5 μg of pFLAG-CMV-4 (Vector), pFLAG-CMV-4-pyrin-WT, pFLAG-CMV-4-pyrin-E148Q, or pFLAG-CMV-4-pyrin-M694V. After incubation with 500 μg/ml G418 (Sigma) in RPMI 1640 medium including 10 % FBS for 4 weeks to generate stable THP-1 cells. Wild-type (WT) and mutated pyrin expressions were confirmed by Western blotting (*inset*, *arrowhead*; *asterisk* is non-specific band). THP-1-derived stable cells expressing WT and mutated pyrin proteins were pre-cultured in 24-well flat-bottomed plates to a final cell density of 2×10^7/ml in a volume of 300 μl of RPMI1640 Medium including 10 % FBS for 8 h at 37 °C in a humidified atmosphere with 5 % CO_2. Then, the culture medium was supplemented with 300 μl of RPMI1640 containing 20 ng/ml LPS. 8 h after medium replacement, the concentrations of IL-1β, IL-6, IL-8, and TNF-α in the culture supernatant were measured by enzyme-linked immunosorbent assay with specific antibodies (BD Biosciences, San Jose, CA, USA). **b** Percentiles of relative suppression of IL-1β, IL-6, IL-8, or TNF-α secretion from THP-1 cells expressing mutated pyrin versus WT pyrin were calculated from triplicate cultures. *A p value <0.05 was considered statistically significant

1β, IL-6, IL-8, or TNF-α with 10 ng/ml LPS stimulation (Fig. 4a); for IL-1β, IL-8, and TNF-α, each cytokine secretion was significantly suppressed by WT pyrin but suppressed much less by M694V pyrin (Fig. 4a, b). In terms of IL-6 secretion from THP-1 cells, there was no significant difference among all the mutations (Fig. 4a, b).

Pyrin affects ERK1/2 phosphorylation of SW982 cells

We found that p38 and ERK 1/2 were spontaneously phosphorylated even when mutated M694V and E148Q pyrin proteins were ectopically expressed in SW982 cells (Fig. 5a, b). ERK1/2 was found to be less phosphorylated when WT pyrin was ectopically expressed in SW982 cells (Fig. 5b). On the other hand, there was no significant phosphorylation in NF-κB p65 for NF-κB activation (Fig. 5c).

Peripheral blood mononuclear cells from FMF patients secreted IL-8 when incubated on a culture plate

We obtained peripheral blood mononuclear cells from five FMF patients with *MEFV* mutations; four patients were E148Q/M694I compound heterozygotes and one patient was an E148Q/E148Q homozygote. We found a significant difference between five FMF patients and five healthy volunteers in terms of IL-8 secretion from mononuclear cells, even when incubated on a culture plate for 6 h (Fig. 6a, b). Peripheral blood mononuclear cells from FMF

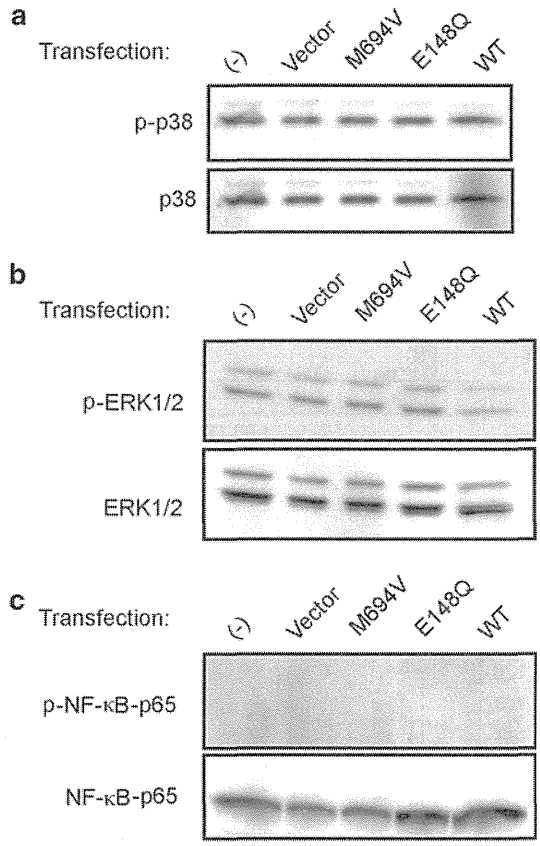

Fig. 5 Western blotting analyses for p38, ERK, and NF-κB pathways. 40 μg of SW982 cell lysates were subjected to SDS-PAGE followed by Western blotting analysis for p38, ERK, and NF-κB pathways. Signals from the same blotting membrane were detected by phospho-p38 MAPK (Thr180/Tyr182) rabbit monoclonal antibody and p38α MAPK rabbit polyclonal antibody for the p38 pathway (**a**), or phospho-p44/42 MAPK (Erk1/2) (Thr202/Tyr204) rabbit monoclonal antibody and p44/42 MAPK (Erk1/2) rabbit monoclonal antibody for the ERK pathway (**b**), or phospho-NF-κB p65 (Ser536) rabbit polyclonal antibody and NF-κB p65 rabbit monoclonal antibodies for the NF-κB pathway (**c**)

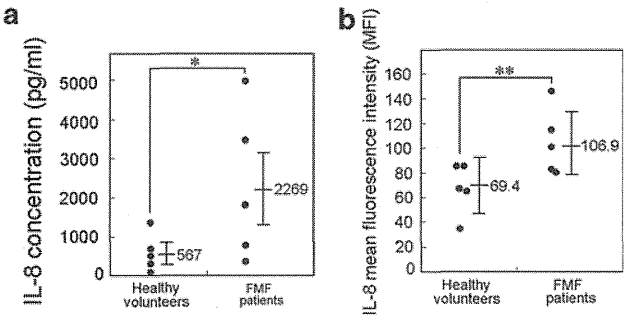

Fig. 6 IL-8 secretion from mononuclear cells from FMF patient with pyrin mutations compared with healthy volunteers. **a** 5×10^5/ml peripheral blood mononuclear cells were incubated in 96-well flat plates with RPMI1640 with 10 % heat-inactivated FBS for 6 h. The supernatants were collected and analyzed for IL-8 concentration (pg/ml) with the Cytometric Bead Array Flex set. **b** 5×10^5/ml mononuclear cells including BD GolgiPlug protein transport inhibitor (BD Biosciences) were incubated under the same conditions as described above. After 6 h of incubation, adherent cells were collected by pipetting. The cells were fixed using a BD Cytofix/Cytoperm solution for 20 min at 4 °C, then fixed cells were permeabilized by washing two times in 1 × BD Perm/Wash buffer. Intracellular IL-8 was stained with FITC-conjugated anti-IL-8 monoclonal antibody and flow cytometric analysis was performed with a FACSCalibur flow cytometer and mean fluorescence intensity (MFI) was calculated. *, ** p values <0.05 and <0.01 were considered statistically significant, respectively

patients were found to exhibit higher IL-8 secretion than those from healthy volunteers (Fig. 6a, b). IL-1β concentrations were at an undetectable level under the same conditions (data not shown).

Discussion

We have investigated the relationship between the main pyrin mutations of FMF patients and the suppression of IL-8 secretion from synovial sarcoma SW982 cells. Pyrin was discovered as a causative gene product of FMF, and E148Q, M694I, and E148Q/M694I mutations of pyrin have been found to be the major mutations of Japanese FMF patients [7, 9]. We constructed mutated-pyrin expression plasmids corresponding to the above mutations (Fig. 1a), and found no apparent difference among WT pyrin and mutated pyrin proteins in terms of expression stability and detergent solubility (Fig. 1b, c). We also found that WT pyrin suppressed IL-8 secretion from SW982 cells, but this was less suppressed by E148Q, M694I, M694V, and E148Q+M694I pyrin in that order, and WT pyrin and mutated pyrin proteins did not affect IL-6 secretion from SW982 cells (Fig. 2). Although it is unusual, compared with normal synovia, for SW982 cells spontaneously to secrete IL-8 without any stimulation, it is likely that a similar model is involved in sterile arthritis, which has been found in FMF patients.

Arthritis is one of the major symptoms of FMF patients [8, 19]. The attacks of FMF arthritis are usually acute inflammatory responses, of which the hallmark in the tissue is self-limiting neutrophil infiltration in synovial stroma [20]. Neutrophils are usually recruited by chemotactic factors such as IL-8, which was shown to be induced by epithelial cells or leukocytes in microbial infection or rheumatoid arthritis [21, 22]. However, sterile inflammation in pleura, peritonea, and synovia, which is common in FMF patients, is thought to occur without any microbial infection or rheumatoid factors [23]. FMF-related sterile inflammation is reported to be triggered by dysregulation of inflammasome, an IL-1β processing platform composed of Nod-like receptor (NLR), ASC, and caspase-1 [24]. It was also reported that NLRC4-inflammasome-related NF-κB activation leads to IL-8 secretion from MEIL-8 cells [12]. The NLRC4-inflammasome-related NF-κB activation

is reported to be inhibited by pyrin [17]. Consistent with this, our results indicated that WT pyrin suppresses IL-8 secretion from SW982 cells (Fig. 2). However, unexpectedly, both ASC and caspase-1 were at undetectable levels in SW982 cells (Fig. 3), suggesting that inflammasome may have been dispensable in the mechanism of suppression of IL-8 secretion from SW982 cells in our experiment (Fig. 3).

To investigate whether pyrin can suppress IL-8 secretion from another cell line, THP-1, monocytic leukemia cells, we generated stable THP-1 cells stably expressing WT pyrin or mutant pyrin proteins such as E148Q, M694V, or vector control. We found that pyrin can suppress IL-8 secretion from THP-1 cells as well as IL-1β and TNF-α (Fig. 4). Because pyrin was reported to inhibit ASC-related inflammasome signaling [15, 16], suppression of IL-1β and TNF-α secretion from THP-1 cells may be inflammasome-dependent. Considering the results from SW982 and THP-1, we speculate that pyrin may contribute to the suppression of IL-8 secretion by an inflammasome-independent pathway.

What kind of signaling pathway does pyrin affect? We performed Western blotting analyses for the p38, ERK, and NF-κB pathways of SW982 cells. Interestingly, we found that p38 and ERK were spontaneously phosphorylated (Fig. 5a, b) and just ERK was less phosphorylated when WT pyrin was ectopically expressed in SW982 cells (Fig. 5b). We also found that NF-κB p65 was not phosphorylated (Fig. 5c). Thus, we speculate that pyrin affects at least the ERK pathway independently of inflammasome.

Notably, peripheral blood mononuclear cells from FMF patients exhibit higher IL-8 secretion than those from healthy volunteers, even when plated on a culture dish (Fig. 6a, b), suggesting that only mechanical stress may affect clinical manifestations of FMF patients.

The most frequent mutation of FMF patients in Middle Eastern countries is reported to be M694V, which is associated with arthritis and severe clinical manifestations [25], whereas no M694V mutation was found among Japanese FMF patients [6–9]. Japanese FMF patients exhibit atypical clinical manifestations, and approximately half of FMF patients exhibit E148Q/M694I compound heterozygosity, E148Q heterozygosity, or M694I homozygosity [9]. As for the clinical significance of our results in correlation with the above description, pyrin-M694V hardly suppressed IL-8 secretion from SW982 and THP-1 cells (Figs. 2, 4, respectively), whereas E148Q, M694I, and E148Q+M694I still had the ability to suppress IL-8 secretion from SW982 cells (Fig. 2).

In conclusion, our data demonstrate that FMF-related mutated pyrin proteins have a low ability to suppress IL-8 secretion from SW982 cells independently of inflammasome. Common mutations in Japanese FMF patients of E148Q, M694I, and E148Q/M694I result in retention of the power to suppress IL-8 secretion from SW982 cells, rather than the M694V mutation, which may explain why atypical clinical manifestations are common in Japanese FMF populations.

Acknowledgments This work was supported by a Grant-in-Aid for Research on Measures for Intractable Diseases from The Ministry of Health, Labor, and Welfare, Japan (to K. M., K. A., and J. M.), and a Grant-in-Aid for Scientific Research on Innovative Areas "Homeostatic Inflammation" of The Ministry of Education, Culture, Sports, Science, and Technology, Japan (J.M.).

Disclosure The authors have no conflict of interest.

References

1. Sohar E, Gafni J, Pras M, Heller H (1967) Familial Mediterranean fever. A survey of 470 cases and review of the literature. Am J Med 43:227–253
2. Stein H, Yarom R, Makin M (1975) Synovitis of familial Mediterranean fever. A histologic and ultrastructural study. Virchows Arch A Pathol Anat Histol 367:263–272
3. The International FMF Consortium (1997) Ancient missense mutations in a new member of the RoRet gene family are likely to cause familial Mediterranean fever. Cell 90:797–807
4. Martinon F, Burns K, Tschopp J (2002) The inflammasome: a molecular platform triggering activation of inflammatory caspases and processing of proIL-β. Mol Cell 10:417–426
5. Chae JJ, Komarow HD, Cheng J, Wood G, Raben N, Liu PP, Kastner DL (2003) Targeted disruption of pyrin, the FMF protein, causes heightened sensitivity to endotoxin and a defect in macrophage apoptosis. Mol Cell 11:591–604
6. Olgun A, Akman S, Kurt I, Tuzun A, Kutluay T (2005) *MEFV* mutations in familial Mediterranean fever: association of M694V homozygosity with arthritis. Rheumatol Int 25:255–259
7. Tsuchiya-Suzuki A, Yazaki M, Nakamura A, Yamazaki K, Agematsu K, Matsuda M, Ikeda S (2009) Clinical and genetic features of familial Mediterranean fever in Japan. J Rheumatol 36:1671–1676
8. Jarjour RA, Dodaki R (2011) Arthritis patterns in familial Mediterranean fever patients and association with M694V mutation. Mol Biol Rep 38:2033–2036
9. Migita K, Uehara R, Nakamura Y, Yasunami M, Tsuchiya-Suzuki A, Yazaki M, Nakamura A, Masumoto J, Yachie A, Furukawa H, Ishibashi H, Ida H, Yamazaki K, Kawakami A, Agematsu K (2012) Familial Mediterranean fever in Japan. Medicine (Baltimore) 91:337–343
10. Gunel-Ozcan A, Sayin DB, Misirlioğlu ED, Güliter S, Yakaryilmaz F, Ensari C (2009) The spectrum of FMF mutations and genotypes in the referrals to molecular genetic laboratory at Kirikkale University in Turkey. Mol Biol Rep 36:757–760
11. Matzner Y, Abedat S, Shapiro E, Eisenberg S, Bar-Gil-Shitrit A, Stepensky P, Calco S, Azar Y, Urieli-Shoval S (2000) Expression of the familial Mediterranean fever gene and activity of the C5a inhibitor in human primary fibroblast cultures. Blood 96:727–731
12. Hasegawa M, Imamura R, Kinoshita T, Matsumoto N, Masumoto J, Inohara N, Suda T (2005) ASC-mediated NF-κB activation leading to interleukin-8 production requires caspase-8 and is inhibited by CLARP. J Biol Chem 280:15122–15130
13. Yoshimura T, Matsushima K, Oppenheim JJ, Leonard EJ (1987) Neutrophil chemotactic factor produced by lipopolysaccharide (LPS)-stimulated human blood mononuclear leukocytes: partial

characterization and separation from interleukin 1 (IL 1). J Immunol 139:788–793
14. Huber AR, Kunkel SL, Todd RF 3rd, Weiss SJ (1991) Regulation of transendothelial neutrophil migration by endogenous interleukin-8. Science 254:99–102
15. Punzi L, Calò L, Plebani M (2002) Clinical significance of cytokine determination in synovial fluid. Crit Rev Clin Lab Sci 39:63–88
16. Dowds TA, Masumoto J, Chen FF, Ogura Y, Inohara N, Núñez G (2003) Regulation of cryopyrin/Pypaf1 signaling by pyrin, the familial Mediterranean fever gene product. Biochem Biophys Res Commun 302:575–580
17. Masumoto J, Dowds TA, Schaner P, Chen FF, Ogura Y, Li M, Zhu L, Katsuyama T, Sagara J, Taniguchi S, Gumucio DL, Núñez G, Inohara N (2003) ASC is an activating adaptor for NF-κB and caspase-8-dependent apoptosis. Biochem Biophys Res Commun 303:69–73
18. Inohara N, Ding L, Chen S, Núñez G (1997) harakiri, a novel regulator of cell death, encodes a protein that activates apoptosis and interacts selectively with survival-promoting proteins Bcl-2 and Bcl-X(L). EMBO J 16:1686–1694
19. Jarjour RA (2010) Familial Mediterranean fever in Syrian patients: *MEFV* gene mutations and genotype-phenotype correlation. Mol Biol Rep 37:1–5
20. Garcia-Gonzalez A, Weisman MH (1992) The arthritis of familial Mediterranean fever. Semin Arthritis Rheum 22:139–150
21. Deleuran B, Lemche P, Kristensen M, Chu CQ, Field M, Jensen J, Matsushima K, Stengaard-Pedersen K (1994) Localisation of interleukin 8 in the synovial membrane, cartilage–pannus junction and chondrocytes in rheumatoid arthritis. Scand J Rheumatol 23:2–7
22. Mukaida N, Harada A, Matsushima K (1998) Interleukin-8 (IL-8) and monocyte chemotactic and activating factor (MCAF/MCP-1), chemokines essentially involved in inflammatory and immune reactions. Cytokine Growth Factor Rev 9:9–23
23. Ben-Chetrit E, Levy M (1998) Familial Mediterranean fever. Lancet 351:659–664
24. Papin S, Cuenin S, Agostini L, Martinon F, Werner S, Beer HD, Grütter C, Grütter M, Tschopp J (2007) The SPRY domain of Pyrin, mutated in familial Mediterranean fever patients, interacts with inflammasome components and inhibits proIL-1β processing. Cell Death Differ 14:1457–1466
25. Brik R, Shinawi M, Kepten I, Berant M, Gershoni-Baruch R (1999) Familial Mediterranean fever: clinical and genetic characterization in a mixed pediatric population of Jewish and Arab patients. Pediatrics 103:e70
26. Masumoto J, Taniguchi S, Ayukawa K, Sarvotham H, Kishino T, Niikawa N, Hidaka E, Katsuyama T, Higuchi T, Sagara J (1999) ASC, a novel 22-kDa protein, aggregates during apoptosis of human promyelocytic leukemia HL-60 cells. J Biol Chem 274:33835–33838

Aicardi-Goutières Syndrome Is Caused by *IFIH1* Mutations

Hirotsugu Oda,[1,2] Kenji Nakagawa,[1] Junya Abe,[1,3] Tomonari Awaya,[1] Masahide Funabiki,[4] Atsushi Hijikata,[5] Ryuta Nishikomori,[1,*] Makoto Funatsuka,[6] Yusei Ohshima,[7] Yuji Sugawara,[8] Takahiro Yasumi,[1] Hiroki Kato,[4,9] Tsuyoshi Shirai,[5] Osamu Ohara,[2,10] Takashi Fujita,[4] and Toshio Heike[1]

Aicardi-Goutières syndrome (AGS) is a rare, genetically determined early-onset progressive encephalopathy. To date, mutations in six genes have been identified as etiologic for AGS. Our Japanese nationwide AGS survey identified six AGS-affected individuals without a molecular diagnosis; we performed whole-exome sequencing on three of these individuals. After removal of the common polymorphisms found in SNP databases, we were able to identify *IFIH1* heterozygous missense mutations in all three. In vitro functional analysis revealed that *IFIH1* mutations increased type I interferon production, and the transcription of interferon-stimulated genes were elevated. *IFIH1* encodes MDA5, and mutant MDA5 lacked ligand-specific responsiveness, similarly to the dominant *Ifih1* mutation responsible for the SLE mouse model that results in type I interferon overproduction. This study suggests that the *IFIH1* mutations are responsible for the AGS phenotype due to an excessive production of type I interferon.

Aicardi-Goutières syndrome (AGS [MIM 225750]) is a rare, genetically determined early-onset progressive encephalopathy.[1] Individuals affected with AGS typically suffer from progressive microcephaly associated with severe neurological symptoms, such as hypotonia, dystonia, seizures, spastic quadriplegia, and severe developmental delay.[2] On brain imaging, AGS is characterized by basal ganglia calcification, white matter abnormalities, and cerebral atrophy.[3,4] Cerebrospinal fluid (CSF) analyses show chronic lymphocytosis and elevated levels of IFN-α and neopterin.[3–5] AGS-affected individuals are often misdiagnosed as having intrauterine infections, such as TORCH syndrome, because of the similarities of these disorders, particularly the intracranial calcifications.[1] In AGS, etiological mutations have been reported in the following six genes: *TREX1* (MIM 606609), which encodes a DNA exonuclease; *RNASEH2A* (MIM 606034), *RNASEH2B* (MIM 610326), and *RNASEH2C* (MIM 610330), which together comprise the RNase H2 endonuclease complex; *SAMHD1* (MIM 606754), which encodes a deoxynucleotide triphosphohydrolase; and *ADAR1* (MIM 146920), which encodes an adenosine deaminase.[6–9] Although more than 90% of AGS-affected individuals harbor etiological mutations in one of these six genes, some AGS-affected individuals presenting with the clinical characteristics of AGS still lack a genetic diagnosis, suggesting the existence of additional AGS-associated genes.[1]

We recently conducted a nationwide survey of AGS in Japan and reported 14 AGS-affected individuals.[10] We have since recruited three other Japanese AGS-affected individuals, and among these 17 individuals, we have identified 11 individuals with etiologic mutations; namely, *TREX1* mutations in six, *SAMHD1* mutations in three, and *RNASEH2A* and *RNASEH2B* mutations in one each. Of the remaining six individuals without a molecular diagnosis, trio-based whole-exome sequencing was performed in three whose parents also agreed to participate in further genome-wide analyses (Figure 1A). Genomic DNA from each individual and the parents was enriched for protein-coding sequences, followed by massively parallel sequencing. The extracted nonsynonymous or splice-site variants were filtered to remove those with minor allele frequencies (MAF) > 0.01 in dbSNP137. To detect de novo variants, any variants observed in family members, listed in Human Genetic Variation Database (HGVD), or with MAF > 0.02 in our in-house exome database were removed. To detect autosomal-recessive (AR), compound heterozygous (CH), or X-linked (XL) variants, those with MAF > 0.05 in our in-house database were removed (Figure S1 available online). All samples were collected with the written informed consents by parents, and the study protocol was approved by the ethical committee of Kyoto University Hospital in accordance with the Declaration of Helsinki.

After common polymorphisms were removed, we identified a total of 40, 18, 89, and 22 candidate variants under the de novo, AR, CH, and XL inheritance models, respectively, that were present in at least one of the three individuals (Table S1). Among them, missense mutations were identified in *IFIH1* (MIM 606951, RefSeq accession

[1]Department of Pediatrics, Kyoto University Graduate School of Medicine, Kyoto 6068507, Japan; [2]Laboratory for Integrative Genomics, RIKEN Center for Integrative Medical Sciences, Yokohama 2300045, Japan; [3]Department of Pediatrics, Kitano Hospital, Tazuke Kofukai Medical Research Institute, Osaka 5308480, Japan; [4]Laboratory of Molecular Genetics, Institute for Virus Research, Kyoto University, Kyoto 6068507, Japan; [5]Department of Bioscience, Nagahama Institute of Bio-Science and Technology, Nagahama 5260829, Japan; [6]Department of Pediatrics, Tokyo Women's Medical University, Tokyo 1628666, Japan; [7]Department of Pediatrics, Faculty of Medical Sciences, University of Fukui, Fukui 9108507, Japan; [8]Department of Pediatrics and Developmental Biology, Graduate School of Medical and Dental Sciences, Tokyo Medical and Dental University, Tokyo 1138510, Japan; [9]Precursory Research for Embryonic Science and Technology (PRESTO), Science and Technology Agency (JST), Kawaguchi 3320012, Japan; [10]Department of Human Genome Research, Kazusa DNA Research Institute, Kisarazu 2920818, Japan
*Correspondence: rnishiko@kuhp.kyoto-u.ac.jp
http://dx.doi.org/10.1016/j.ajhg.2014.06.007.

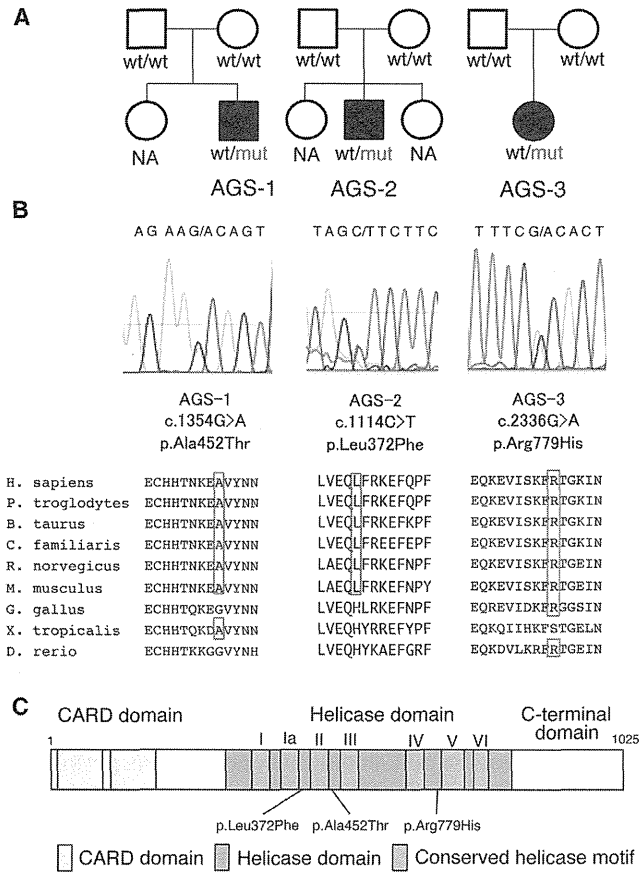

Figure 1. Pedigree Information for the AGS-Affected Individuals and Details of the *IFIH1* Mutations Identified

(A) The pedigrees of the three families indicating the AGS probands.

(B) Sanger sequencing chromatograms of the three *IFIH1* mutations found in the AGS-affected individuals. The locations of these mutations in the amino acid sequence of the MDA5 protein are shown in alignment with the conserved amino acid sequences from several species. This alignment was obtained via ClustalW2. The amino acids that are conserved with human are circled in red.

(C) The MDA5 protein domain structure with the amino acid substitutions observed in these AGS-affected individuals.

number NM_022168.2), which encodes MDA5 (RefSeq NP_071451.2). These missense mutations are c.1354G>A (p.Ala452Thr) in AGS-1; c.1114C>T (p.Leu372Phe) in AGS-2; and c.2336G>A (p.Arg779His) in AGS-3 (Figure 1B). None of the mutations are found in HGVD, including the 1,208 Japanese samples, or our in-house exome database of 312 Japanese individuals. Multiple-sequence alignment by ClustalW2 revealed that each of the amino acids affected by these mutations are conserved among mammals (Figure 1B). The subsequent amino acid alterations were all suggested to be disease causing in at least one of the four function-prediction programs used (Table 1). None of the other genes identified in the de novo inheritance model, or any of the genes identified in the other three inheritance models, were mutated in all three individuals. The *IFIH1* mutations identified were validated by Sanger sequencing. The other coding exons of *IFIH1* were also examined by Sanger sequencing, and no other mutations were found.

MDA5 is one of the cytosolic pattern recognition receptors that recognizes double-stranded RNA (dsRNA).[11] MDA5 consists of N-terminal tandem CARD domains, a central helicase domain, and a C-terminal domain (Figure 1C). When bound to dsRNA, MDA5 forms a closed, C-shaped ring structure around the dsRNA stem and excludes the tandem CARD as well as creates filamentous oligomer on dsRNA.[12] It is hypothesized that the tandem CARD interacts each other and activates MAVS on the mitochondrial outer membrane. Oligomerization of MAVS induces TBK1 activation, IRF3 phosphorylation, and induction of type I interferon transcription, resulting in the activation of a large number of interferon-stimulated genes (ISGs).

The neurological findings of the individuals with these *IFIH1* mutations are typical of AGS (Table S2). They were born with appropriate weights for their gestational ages without any signs of intrauterine infection. However, they all demonstrated severe developmental delay in early infancy associated with progressive microcephaly. No arthropathy, hearing loss, or ophthalmological problems were observed. As for extraneural features, all three individuals had at least one of the following autoimmune features: positivity for autoantibodies, hyperimmunoglobulinemia, hypocomplementemia, and thrombocytopenia. Notably, none of the individuals with *IFIH1* mutations had chilblain lesions, although all the five individuals with *TREX1* mutations and two of the three individuals with *SAMHD1* mutations in the Japanese AGS cohort showed chilblain lesions.[10] Individuals with *SAMHD1* mutations and *IFIH1* mutations both show autoimmune features; however, chilblain lesions have been observed only in individuals with *SAMHD1* mutations.[10]

To predict the effects of the identified amino acid substitutions on MDA5, three-dimensional model structures of MDA5 mutants were generated from the crystal structure of human MDA5-dsRNA complex[12] (Protein Data Bank [PDB] code 4gl2), using PyMOL (Schroedinger) and MOE (Chemical Computing Group) (Figure S2A). The oligomeric model of MDA5 was generated using the electron microscopy imaging data of MDA5 filament lacking CARD domain[13] (Electron Microscopic Data Bank [EMDB] code 5444) (Figure S2B). The three amino acid substitutions in the AGS-affected individuals are all located within the helicase domain (Figures 1C and S2A). Because Ala452 directly contacts the dsRNA ribose O2′ atom, the p.Ala452Thr substitution probably affects the binding affinity to dsRNA due to an atomic repulsion between the side chain of Thr452 and the dsRNA O2′ atom (Figures S2C and S2D). Leu372 is located adjacent to the ATP binding pocket, and the p.Leu372Phe substitution could increase the side chain volume of the binding pocket, affecting its ATP hydrolysis activity (Figures S2E and S2F). In our oligomeric model, Arg779 is located at the interface between the two monomers, which is consistent with the

Table 1. Functional Predictions of the *IFIH1* Variants

Individuals	Nucleotide Change	Amino Acid Change	SIFT	PolyPhen2	Mutation Taster	PROVEAN
AGS-1	c.1354G>A	p.Ala452Thr	tolerated	benign	disease causing	neutral
AGS-2	c.1114C>T	p.Leu372Phe	tolerated	probably damaging	disease causing	neutral
AGS-3	c.2336G>A	p.Arg779His	tolerated	probably damaging	disease causing	deleterious

The potential functional effects of the *IFIH1* variants identified in the AGS-affected individuals were predicted via SIFT, PolyPhen2, Mutation Taster, and PROVEAN.

recent report showing that Lys777, close to Arg779, is in close proximity to the adjacent monomer.[12] Furthermore, in our model, Arg779 is in close to Asp572 on the surface of the adjacent monomer. We speculate that losing the positive charge due to the p.Arg779His substitution would possibly affect the electrostatic interaction between the MDA5 monomers (Figures S2G and S2H).

To connect the identified *IFIH1* mutations with the AGS phenotype, we examined the type I interferon signature in the individuals by performing quantitative RT-PCR (qRT-PCR) of seven ISGs.[14] Peripheral blood mononuclear cells (PBMCs) from the three AGS-affected individuals showed upregulation of ISG transcription (Figure 2), confirming the type I interferon signature in the individuals with *IFIH1* mutations.

To elucidate the disease-causing capability of the identified *IFIH1* mutations, three FLAG-tagged *IFIH1* mutant plasmids containing these mutations were constructed via site-directed mutagenesis. These plasmids were transiently expressed on human hepatoma cell line Huh7 and the *IFNB1* promoter activity as well as endogenous expression of *IFIT1* (MIM 147690) was measured 48 hr after transfection.[15] The three mutant plasmids activated the *IFNB1* promoter in Huh7 cells more strongly than the wild MDA5 and nearby missense variants reported in dbSNP (Figures 3 and S3). The upregulation of endogenous *IFIT1* was also observed in the transfected cells (Figure S4), suggesting that these AGS mutations enhance the intrinsic activation function of MDA5. Recent genome-wide association studies (GWASs) showed association of the *IFIH1* with various autoimmune diseases, such as systemic lupus erythematosus (SLE), type I diabetes, psoriasis, and vitiligo.[16–19] We examined *IFNB1* promoter activity induced by the c.2836G>A (p.Ala946Thr) polymorphism (rs1990760) identified in the GWASs. Although the c.2836G>A polymorphism partially activated the promoter activity, the induced activity was lower than those of the AGS-derived mutants. In addition, the dominantly inherited SLE mouse model in the ENU-treated mouse colony is reported to have the *Ifih1* mutation, c.2461G>A (p.Gly821Ser).[15] These observations suggest that *IFIH1* has strong association with various autoimmune diseases, especially SLE, which also has a type I interferon signature.[20] Because alteration of *TREX1* has been reported to cause AGS as well as SLE,[21] it seems quite plausible for *IFIH1* to also be involved in both AGS and SLE. Interestingly, all the individuals identified with *IFIH1* mutations had autoantibodies, suggesting the contribution of *IFIH1* mutations to autoimmune phenotypes.

To further delineate the functional consequences of the three *IFH1* mutations, we measured the ligand-specific *Ifnb* mRNA induction by stimulating *Ifih1*^{null} mouse embryonic fibroblasts (MEFs) reconstituted with retrovirus expressing the *IFIH1* mutants by an MDA5-specific ligand, encephalomyocarditis virus (EMCV).[22] None of the MEF cells expressing the three mutant *IFIH1* responded to the EMCV, which suggested that the MDA5 variants lacked the ligand-specific responsiveness. The response of the three AGS mutants against the MDA5-specific EMCV was similar to that of the p.Gly821Ser variant reported in the dominantly inherited SLE mouse model with type I interferon overproduction[15] (Figures 4 and S5).

During the revision of this manuscript, Rice et al. identified nine individuals with *IFIH1* mutations, including the c.2336G>A mutation we identified, in a spectrum of neuroimmunological features consistently associated with enhanced type I interferon states including AGS.[23] Although we agree that the *IFIH1* mutations cause constitutive type I interferon activation, Rice et al. show that the mutated MDA5 proteins maintain ligand-induced responsiveness, which was not the case in our study. Because we measured the ligand-specific responsiveness of MDA5 in different experimental conditions, further analysis remains to be performed to reveal the biochemical mechanism of interferon overproduction by the mutated MDA5.

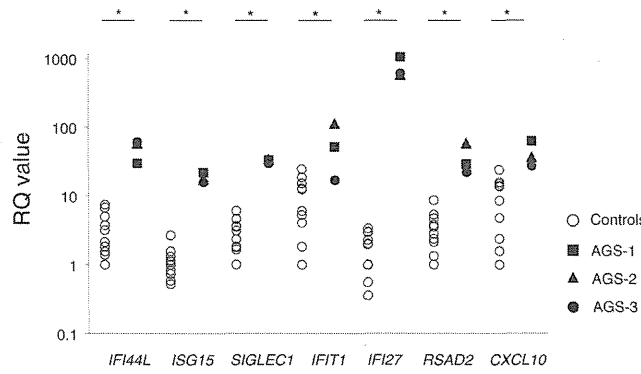

Figure 2. Quantitative RT-PCR of a Panel of Seven ISGs in PBMCs Obtained from the *IFIH1*-Mutated Individuals and Healthy Control Subject

qRT-PCR was performed as previously described.[15] The relative abundance of each transcript was normalized to the expression level of β-actin. Taqman probes used were the same as previous report,[14] except for *ACTB* (MIM 102630). Individual data were shown relative to a single calibrator (control 1). The experiment was performed in triplicate. Statistical significance was determined by Mann-Whitney U test, *$p < 0.05$.

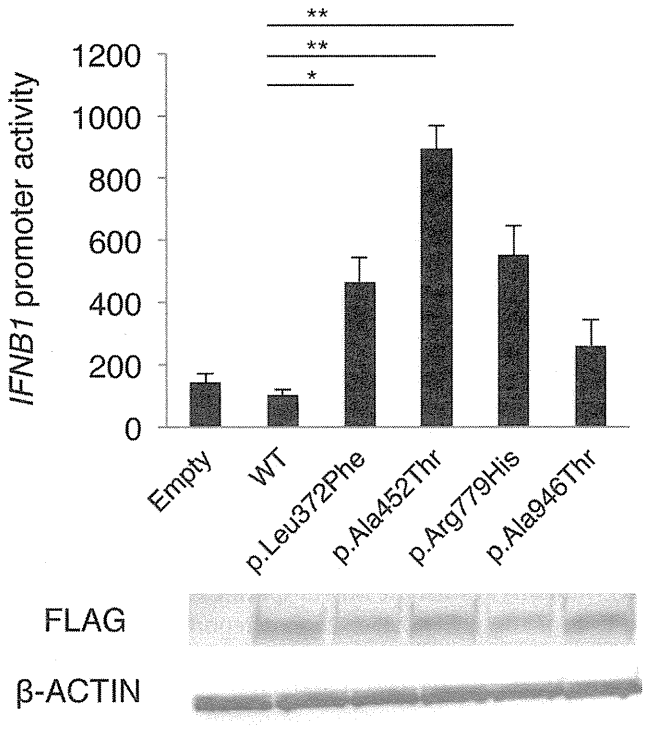

Figure 3. The Effects of the Three MDA5 Variants on *IFNB1* Expression

Huh7 cells were transfected with a reporter gene containing *IFNB1* promoter (p-55C1B Luc), an empty vector (BOS), and expression vectors for FLAG-tagged human wild-type *IFIH1*, c.2836G>A polymorphism (p.Ala946Thr) in the GWASs, and the identified *IFIH1* mutants. Luciferase activity was measured 48 hr after transfection, and the MDA5 protein accumulation was examined by immunoblotting as previously described.[15] FLAG indicates the accumulation of FLAG-tagged MDA5. Each experiment was performed in triplicate and data are mean ± SEM. Shown is a representative of two with consistent results. Statistical significance was determined by Student's t test. *$p < 0.05$, **$p < 0.01$.

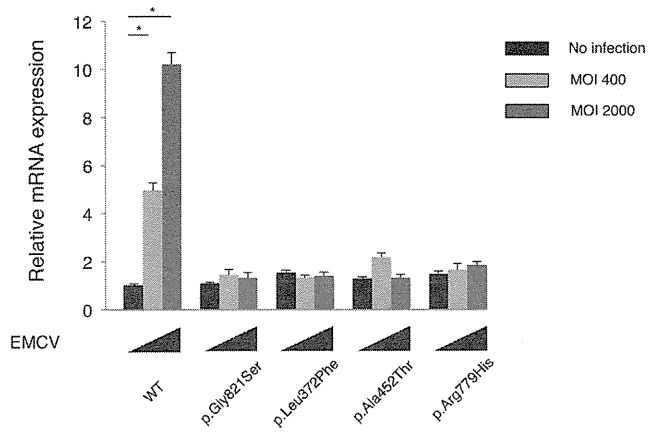

Figure 4. *Ifnb* mRNA Levels in *Ifih1*-Deficient MEFs Expressing *IFIH1* Mutants

The MEFs were infected with retroviruses encoding mouse wild-type *Ifih1*, mouse *Ifih1* with c.2461G>A (p.Gly821Ser) (RefSeq NM_027835.3) mutation, or the three AGS mutants of human *IFIH1*. At 48 hr after the retroviral infection, these MEFs were infected with indicated multiplicity of infection (MOI) of EMCV for 6 hr, and *Ifnb* mRNA levels were measured by qRT-PCR. The relative abundance of each transcript was normalized to the expression level of 18S ribosomal RNA. Data are shown as mean ± SEM of triplicate samples. Shown is a representative of two independent experiments. Statistical significance was determined by Student's t test, *$p < 0.001$. The expression of the retrovirally transduced FLAG-tagged constructs was confirmed by immunoblotting (Figure S5).

In conclusion, we identified mutations in *IFIH1* as a cause of AGS. The individuals with the *IFIH1* mutations showed encephalopathy typical of AGS as well as the type I interferon signature with autoimmune phenotypes, but lacked the chilblains. Further analysis remains to elucidate the mechanism of how the *IFIH1* mutations identified in AGS cause the type I interferon overproduction.

Supplemental Data

Supplemental Data include five figures and two tables and can be found with this article online at http://dx.doi.org/10.1016/j.ajhg.2014.06.007.

Acknowledgments

We are very grateful to Y. Takaoka (Kyoto University) and E. Abe (RIKEN Center for Integrative Medical Sciences) for their technical assistance on Sanger sequencing, to E. Hirano (Kyoto University) for her technical assistance on functional analyses of the AGS mutants, to M. Takazawa (Kazusa DNA Research Institute) for his contribution to exome data analysis, and to T. Taylor for his critical reading of the manuscript. This work was supported by the Platform for Drug Discovery, Informatics, and Structural Life Science from the Ministry of Education, Culture, Sports, Science and Technology, Japan. This work was supported by Grants-in-aid for Scientific Research from the Japanese Ministry of Health, Labor and Welfare and the Japanese Ministry of Education, Culture, Sports, Science, Technology (MEXT).

Received: March 1, 2014
Accepted: June 11, 2014
Published: July 3, 2014

Web Resources

The URLs for the data presented herein are as follows:

Burrows-Wheeler Aligner, http://bio-bwa.sourceforge.net/
ClustalW2, http://www.ebi.ac.uk/Tools/msa/clustalw2/
dbSNP, http://www.ncbi.nlm.nih.gov/projects/SNP/
EMDataBank, http://www.emdatabank.org/index.html
GATK, http://www.broadinstitute.org/gatk/
Human Genetic Variation Database (HGVD), http://www.genome.med.kyoto-u.ac.jp/SnpDB/
MutationTaster, http://www.mutationtaster.org/
Online Mendelian Inheritance in Man (OMIM), http://www.omim.org/
PolyPhen-2, http://www.genetics.bwh.harvard.edu/pph2/
PROVEAN, http://provean.jcvi.org/index.php
RCSB Protein Data Bank, http://www.rcsb.org/pdb/home/home.do
RefSeq, http://www.ncbi.nlm.nih.gov/RefSeq
SIFT, http://sift.bii.a-star.edu.sg/

References

1. Chahwan, C., and Chahwan, R. (2012). Aicardi-Goutieres syndrome: from patients to genes and beyond. Clin. Genet. *81*, 413–420.
2. Ramantani, G., Kohlhase, J., Hertzberg, C., Innes, A.M., Engel, K., Hunger, S., Borozdin, W., Mah, J.K., Ungerath, K., Walkenhorst, H., et al. (2010). Expanding the phenotypic spectrum of lupus erythematosus in Aicardi-Goutières syndrome. Arthritis Rheum. *62*, 1469–1477.
3. Orcesi, S., La Piana, R., and Fazzi, E. (2009). Aicardi-Goutieres syndrome. Br. Med. Bull. *89*, 183–201.
4. Rice, G., Patrick, T., Parmar, R., Taylor, C.F., Aeby, A., Aicardi, J., Artuch, R., Montalto, S.A., Bacino, C.A., Barroso, B., et al. (2007). Clinical and molecular phenotype of Aicardi-Goutieres syndrome. Am. J. Hum. Genet. *81*, 713–725.
5. Blau, N., Bonafé, L., Krägeloh-Mann, I., Thöny, B., Kierat, L., Häusler, M., and Ramaekers, V. (2003). Cerebrospinal fluid pterins and folates in Aicardi-Goutières syndrome: a new phenotype. Neurology *61*, 642–647.
6. Crow, Y.J., Hayward, B.E., Parmar, R., Robins, P., Leitch, A., Ali, M., Black, D.N., van Bokhoven, H., Brunner, H.G., Hamel, B.C., et al. (2006). Mutations in the gene encoding the 3′-5′ DNA exonuclease TREX1 cause Aicardi-Goutières syndrome at the AGS1 locus. Nat. Genet. *38*, 917–920.
7. Crow, Y.J., Leitch, A., Hayward, B.E., Garner, A., Parmar, R., Griffith, E., Ali, M., Semple, C., Aicardi, J., Babul-Hirji, R., et al. (2006). Mutations in genes encoding ribonuclease H2 subunits cause Aicardi-Goutières syndrome and mimic congenital viral brain infection. Nat. Genet. *38*, 910–916.
8. Rice, G.I., Bond, J., Asipu, A., Brunette, R.L., Manfield, I.W., Carr, I.M., Fuller, J.C., Jackson, R.M., Lamb, T., Briggs, T.A., et al. (2009). Mutations involved in Aicardi-Goutières syndrome implicate SAMHD1 as regulator of the innate immune response. Nat. Genet. *41*, 829–832.
9. Rice, G.I., Kasher, P.R., Forte, G.M., Mannion, N.M., Greenwood, S.M., Szynkiewicz, M., Dickerson, J.E., Bhaskar, S.S., Zampini, M., Briggs, T.A., et al. (2012). Mutations in ADAR1 cause Aicardi-Goutières syndrome associated with a type I interferon signature. Nat. Genet. *44*, 1243–1248.
10. Abe, J., Nakamura, K., Nishikomori, R., Kato, M., Mitsuiki, N., Izawa, K., Awaya, T., Kawai, T., Yasumi, T., Toyoshima, I., et al. (2014). A nationwide survey of Aicardi-Goutieres syndrome patients identifies a strong association between dominant TREX1 mutations and chilblain lesions: Japanese cohort study. Rheumatology *53*, 448–458.
11. Yoneyama, M., and Fujita, T. (2009). RNA recognition and signal transduction by RIG-I-like receptors. Immunol. Rev. *227*, 54–65.
12. Wu, B., Peisley, A., Richards, C., Yao, H., Zeng, X., Lin, C., Chu, F., Walz, T., and Hur, S. (2013). Structural basis for dsRNA recognition, filament formation, and antiviral signal activation by MDA5. Cell *152*, 276–289.
13. Berke, I.C., Yu, X., Modis, Y., and Egelman, E.H. (2012). MDA5 assembles into a polar helical filament on dsRNA. Proc. Natl. Acad. Sci. USA *109*, 18437–18441.
14. Rice, G.I., Forte, G.M., Szynkiewicz, M., Chase, D.S., Aeby, A., Abdel-Hamid, M.S., Ackroyd, S., Allcock, R., Bailey, K.M., Balottin, U., et al. (2013). Assessment of interferon-related biomarkers in Aicardi-Goutières syndrome associated with mutations in TREX1, RNASEH2A, RNASEH2B, RNASEH2C, SAMHD1, and ADAR: a case-control study. Lancet Neurol. *12*, 1159–1169.
15. Funabiki, M., Kato, H., Miyachi, Y., Toki, H., Motegi, H., Inoue, M., Minowa, O., Yoshida, A., Deguchi, K., Sato, H., et al. (2014). Autoimmune disorders associated with gain of function of the intracellular sensor MDA5. Immunity *40*, 199–212.
16. Smyth, D.J., Cooper, J.D., Bailey, R., Field, S., Burren, O., Smink, L.J., Guja, C., Ionescu-Tirgoviste, C., Widmer, B., Dunger, D.B., et al. (2006). A genome-wide association study of nonsynonymous SNPs identifies a type 1 diabetes locus in the interferon-induced helicase (IFIH1) region. Nat. Genet. *38*, 617–619.
17. Gateva, V., Sandling, J.K., Hom, G., Taylor, K.E., Chung, S.A., Sun, X., Ortmann, W., Kosoy, R., Ferreira, R.C., Nordmark, G., et al. (2009). A large-scale replication study identifies TNIP1, PRDM1, JAZF1, UHRF1BP1 and IL10 as risk loci for systemic lupus erythematosus. Nat. Genet. *41*, 1228–1233.
18. Strange, A., Capon, F., Spencer, C.C., Knight, J., Weale, M.E., Allen, M.H., Barton, A., Band, G., Bellenguez, C., Bergboer, J.G., et al.; Genetic Analysis of Psoriasis Consortium & the Wellcome Trust Case Control Consortium 2 (2010). A genome-wide association study identifies new psoriasis susceptibility loci and an interaction between HLA-C and ERAP1. Nat. Genet. *42*, 985–990.
19. Jin, Y., Birlea, S.A., Fain, P.R., Ferrara, T.M., Ben, S., Riccardi, S.L., Cole, J.B., Gowan, K., Holland, P.J., Bennett, D.C., et al. (2012). Genome-wide association analyses identify 13 new susceptibility loci for generalized vitiligo. Nat. Genet. *44*, 676–680.
20. Bennett, L., Palucka, A.K., Arce, E., Cantrell, V., Borvak, J., Banchereau, J., and Pascual, V. (2003). Interferon and granulopoiesis signatures in systemic lupus erythematosus blood. J. Exp. Med. *197*, 711–723.
21. Lee-Kirsch, M.A., Gong, M., Chowdhury, D., Senenko, L., Engel, K., Lee, Y.A., de Silva, U., Bailey, S.L., Witte, T., Vyse, T.J., et al. (2007). Mutations in the gene encoding the 3′-5′ DNA exonuclease TREX1 are associated with systemic lupus erythematosus. Nat. Genet. *39*, 1065–1067.
22. Kato, H., Takeuchi, O., Sato, S., Yoneyama, M., Yamamoto, M., Matsui, K., Uematsu, S., Jung, A., Kawai, T., Ishii, K.J., et al. (2006). Differential roles of MDA5 and RIG-I helicases in the recognition of RNA viruses. Nature *441*, 101–105.
23. Rice, G.I., del Toro Duany, Y., Jenkinson, E.M., Forte, G.M., Anderson, B.H., Ariaudo, G., Bader-Meunier, B., Baildam, E.M., Battini, R., Beresford, M.W., et al. (2014). Gain-of-function mutations in IFIH1 cause a spectrum of human disease phenotypes associated with upregulated type I interferon signaling. Nat. Genet. *46*, 503–509.

OPEN ACCESS
CellPress

Cell Reports
Report

Single-Cell Imaging of Caspase-1 Dynamics Reveals an All-or-None Inflammasome Signaling Response

Ting Liu,[1] Yoshifumi Yamaguchi,[1,2,*] Yoshitaka Shirasaki,[3] Koichi Shikada,[1] Mai Yamagishi,[3] Katsuaki Hoshino,[4,5,6] Tsuneyasu Kaisho,[5,6,12] Kiwamu Takemoto,[2,7] Toshihiko Suzuki,[8] Erina Kuranaga,[9] Osamu Ohara,[3,10] and Masayuki Miura[1,11,*]

[1]Department of Genetics, Graduate School of Pharmaceutical Sciences, The University of Tokyo, Bunkyo-ku, Tokyo 113-0033, Japan
[2]PRESTO, Japan Science and Technology Agency, Chiyoda-ku, Tokyo 102-0076, Japan
[3]Laboratory for Integrative Genomics, RIKEN Center for Integrative Medical Sciences (IMS-RCAI), Yokohama, Kanagawa 230-0045, Japan
[4]Department of Immunology, Faculty of Medicine, Kagawa University, Kita-gun, Kagawa 761-0793, Japan
[5]Laboratory for Immune Regulation, World Premier International Research Center Initiative Immunology Frontier Research Center, Osaka University, Suita, Osaka 565-0861, Japan
[6]Laboratory for Host Defense, RIKEN Research Center for Allergy and Immunology, Yokohama, Kanagawa 230-0045, Japan
[7]Department of Physiology, Graduate School of Medicine, Yokohama City University, Yokohama, Kanagawa 236-0004, Japan
[8]Department of Molecular Bacteriology and Immunology, Graduate School of Medicine, University of the Ryukyus, Nakagami-gun, Okinawa 903-0125, Japan
[9]Laboratory for Histogenetic Dynamics, RIKEN Center for Developmental Biology, Chuo-ku, Kobe 650-0047, Japan
[10]Department of Human Genome Research, Kazusa DNA Research Institute, Kisarazu, Chiba 292-0818, Japan
[11]CREST, Japan Science and Technology Agency, Chiyoda-ku, Tokyo 102-0076, Japan
[12]Present address: Department of Immunology, Institute of Advanced Medicine, Wakayama Medical University, 811-1 Kimiidera, Wakayama, Wakayama 641-8509, Japan
*Correspondence: bunbun@mol.f.u-tokyo.ac.jp (Y.Y.), miura@mol.f.u-tokyo.ac.jp (M.M.)
http://dx.doi.org/10.1016/j.celrep.2014.07.012

SUMMARY

Inflammasome-mediated caspase-1 activation is involved in cell death and the secretion of the proinflammatory cytokine interleukin-1β (IL-1β). Although the dynamics of caspase-1 activation, IL-1β secretion, and cell death have been examined with bulk assays in population-level studies, they remain poorly understood at the single-cell level. In this study, we conducted single-cell imaging using a genetic fluorescence resonance energy transfer sensor that detects caspase-1 activation. We determined that caspase-1 exhibits all-or-none (digital) activation at the single-cell level, with similar activation kinetics irrespective of the type of inflammasome or the intensity of the stimulus. Real-time concurrent detection of caspase-1 activation and IL-1β release demonstrated that dead macrophages containing activated caspase-1 release a local burst of IL-1β in a digital manner, which identified these macrophages as the main source of IL-1β within cell populations. Our results highlight the value of single-cell analysis in enhancing understanding of the inflammasome system and chronic inflammatory diseases.

INTRODUCTION

Macrophages (MΦs) play crucial roles in homeostasis by clearing dead cells and connecting innate immunity with adaptive immunity (Mosser and Edwards, 2008). When MΦs detect pathogen-associated molecular patterns (PAMPs) derived from infection or damage-associated molecular patterns (DAMPs) originating from injured tissues, they secrete various types of cytokines to induce inflammation or tissue repair. Interleukin-1β (IL-1β) is a key cytokine that evokes an inflammatory response, and its secretion is mainly regulated by caspase-1, a member of the cysteine-protease family of caspases (Denes et al., 2012).

Caspase-1 is synthesized as an inactive zymogen and then activated via proteolytic cleavage, a process regulated by intracellular multiprotein complexes called inflammasomes (Martinon et al., 2002; Rathinam et al., 2012); the inflammasomes detect PAMPs and DAMPs by using distinct intracellular pattern-recognition receptors such as NLRP3 (Nod-like receptor family, pyrin domain containing 3), NLRC4 (Nod-like receptor family, CARD domain containing 4), and AIM2 (absent in melanoma 2) (Martinon et al., 2002; Rathinam et al., 2012). When PAMPs or DAMPs are detected, procaspase-1 is recruited directly through interactions between the pattern-recognition receptors and procaspase-1 or indirectly through adaptor proteins such as ASC (apoptosis-associated speck-like protein containing CARD) (Schroder and Tschopp, 2010). The recruited procaspase-1 is activated through autoproteolytic cleavage mediated by proximity-induced multimerization. In addition to regulating proinflammatory cytokines, caspase-1 activation has been shown to cause cell death (Miura et al., 1993). In certain cases, caspase-1 is necessary for the execution of necrotic inflammatory cell death, called pyroptosis, in MΦs in response to intracellular bacterial infection (Fink and Cookson, 2005; Miao et al., 2010). However, in other cases, although caspase-1 is activated in response to various PAMPs or DAMPs, deleting or inhibiting caspase-1 is

insufficient for preventing cell death (Broz et al., 2010; Pierini et al., 2012).

Given the aforementioned studies, the activation of most inflammasomes is considered to typically converge on caspase-1 activation, which couples the secretion of the proinflammatory cytokine IL-1β and cell death. However, most of the information on inflammasomes and caspase-1 has been obtained from population-level studies conducted using bulk assays such as western blotting and ELISA, mainly because of technical limitations and because of the unique characteristics of caspase-1 such as rapid secretion after activation and rapid inactivation (Keller et al., 2008; Walsh et al., 2011). Emerging evidence suggests that population data do not faithfully reflect how single cells respond to stimuli (Tay et al., 2010). Thus, the mechanism through which individual cells activate caspase-1 by means of distinct inflammasomes and secrete IL-1β in response to inflammatory stimuli remains unclear. Determining signaling dynamics at the single-cell level not only expands the general understanding of how biological systems work but also complements in vivo studies that examine cells residing in complex contexts (Tay et al., 2010). Single-cell measurement of caspase-1 activity at high spatiotemporal resolution is required to fully understand the dynamics of caspase-1 activation and the direct relationship between caspase-1 activation and its associated outcomes, IL-1β secretion and cell death.

To monitor caspase-1 activity at the single-cell level, we developed SCAT1, a genetically encoded fluorescent sensor for detecting caspase-1 activation based on fluorescence resonance energy transfer (FRET). Using peritoneal MΦs (PMΦs) obtained from transgenic mice expressing SCAT1, we determined that caspase-1 is activated in a digital manner at the single-cell level in response to various types of inflammasomes. Interestingly, the kinetics of caspase-1 activation was similar regardless of the strength and type of stimuli. Moreover, by combining the SCAT1 system and a newly developed technique to measure protein secretion at single-cell resolution, we identified dying MΦs that contained activated caspase-1 as the source of secreted IL-1β in PMΦ populations.

RESULTS

Real-Time Detection of Caspase-1 Activation through the NLRP3 Inflammasome with SCAT1, a Genetically Encoded Probe Developed for Monitoring Caspase-1 Activation

Probes based on FRET technology can provide critical information on the dynamics and activities of endogenous enzymes in living cells (Aoki et al., 2013). We previously generated a genetically encoded probe called SCAT3 (sensor for caspase-3 activation based on FRET) and monitored apoptotic caspase-3 activation in vitro and in vivo (Kuranaga et al., 2011; Nakajima et al., 2011; Takemoto et al., 2003, 2007; Yamaguchi et al., 2011). SCAT comprises 2 fluorescent proteins—enhanced cyan fluorescent protein (ECFP) and Venus—that are connected by a linker sequence that contains caspase cleavage sites (Figure 1A). Upon caspase activation, the linker is cleaved and the FRET between ECFP and Venus is disrupted, which can be detected in real time with fluorescence microscopy. To detect real-time activation of caspase-1, we constructed SCAT1 containing YVAD (a consensus peptide sequence preferentially cleaved by caspase-1) in its linker sequence instead of the DEVD sequence present in SCAT3 (Figure 1A).

The results of in vitro cleavage assays demonstrated that SCAT1 was preferentially cleaved by activated human caspase-1 (Figure S1A). Notably, SCAT1 was barely processed by activated human caspase-4 and caspase-5, which represent potential functional orthologs of murine caspase-11. The specificity of SCAT1 cleavage upon caspase-1 activation was also confirmed in living cells with the caspase-1-specific inhibitor z-YVAD-fmk or by genetic deletion of caspase-1/11 (Figure S1B; see below for a detailed explanation). We generated a gene-targeting mouse line in which the CAG-promoter-loxP-STOP-loxP-SCAT1 gene cassette was knocked into the Rosa26 locus. In this knockin mouse line, SCAT1 expression depended on Cre recombinase expression (Figure S1C); by mating these mice with mice that ubiquitously expressed Cre, we generated mice that expressed SCAT1 in all tissues. We obtained peritoneal MΦs (PMΦs) expressing SCAT1 from these mice. The possibility that overexpressed SCAT1, an exogenous substrate of caspase-1, might prevent the endogenous function of caspase-1 was excluded by our observation that IL-1β secretion and caspase-1 cleavage occurred similarly in PMΦs derived from SCAT1$^-$ (wild-type) and SCAT1$^+$ mice after inflammasome-activation stimulated with lipopolysaccharide (LPS) + ATP or poly(dA:dT) (Figures S1D and S1E).

Various pathogenic, endogenous, and environmental stimuli can activate the NLRP3 inflammasome after priming with LPS or other Toll-like receptor ligands (Latz et al., 2013). We examined whether SCAT1 can enable real-time detection of caspase-1 activation induced by canonical activators of the NLRP3 inflammasome at the single-cell level. PMΦs collected from SCAT1 knockin mice were stimulated with an environmental danger signal (silica crystals) after LPS priming and were observed continuously under a confocal microscope to monitor the time course of changes in SCAT1 (Venus and ECFP) intensities. The SCAT1 Venus/ECFP (V/C) ratio decreased rapidly and dramatically (Figures 1B and 1C; Movie S1) in some of the cells after stimulation, indicating that caspase-1 was activated; the time of caspase-1 activation varied among cells (Figures S2A and S2B). Moreover, adding the caspase-1-specific inhibitor z-YVAD-fmk abolished the dramatic reduction in the SCAT1 V/C ratio and the cleavage of SCAT1 (Figures 1B, 1C, S1B, S2A, and S2B; Movie S1), indicating that SCAT1 accurately detected caspase-1 activation. We also confirmed that apoptotic caspases were not activated in PMΦs stimulated with LPS + silica; SCAT3, the indicator of caspase-3 activation, did not detect apoptotic activation of caspases in these PMΦs (Figure S2C).

Time-lapse imaging showed that SCAT1 fluorescence disappeared after caspase-1 activation, but the fluorescence was lost even when caspase-1 activation was prevented by its inhibitor (Figure 1B). This loss of fluorescence indicated cell death accompanying membrane rupture because it coincided with the cells becoming positive for TO-PRO-3 or propidium iodide staining (Figure 1D; Movie S1). These data indicated that SCAT1 can faithfully detect NLRP3 inflammasome-induced activation of caspase-1 and subsequent cell death in real time at the single-cell level. Interestingly, the dynamics of SCAT1 V/C ratios